FREEZE CASTED POROUS CERAMICS

by

SANTIAGO GIL DURÁN

A dissertation submitted to Universidad EAFIT for the Degree of

DOCTOR OF PHILOSOPHY

School of Engineering

Universidad EAFIT

January 2020

Preface and Declaration

The work described in this dissertation was carried out at Universidad Eafit between July 2014 and January 2020.

I would like to thank my supervisor Professor Alex Ossa for his invaluable patience and support. Thanks to Professor Dwayne Arola from the Materials Science and Engineering Department at the University of Washington for allowing me to join his research group during the internship.

Support for this study was provided in part by a grant from Universidad Eafit and by Departamento Administrativo de Ciencia Tecnología e Innovación, Colciencias by contract 0210-2013.

This dissertation is the result of my own work, except where specific reference has been made to the work of others. No part of the work has been, or is currently being, submitted for any degree, diploma or other qualification.

FREEZE CASTED POROUS CERAMICS

Santiago Gil-Duran

Summary

Scientists have explored different manufacturing methods aiming at obtaining synthetic materials with controlled porosity, among them, Freeze Casting allows a control of the pore characteristics formed within the material by setting process variables like type of medium, particle size, solid content, inclusion of additives, freezing rate, etc. Despite of all the knowledge obtained about freeze casting, there still remain some questions to solve regarding processing-structure relationships, specifically the relations between cooling patterns during freezing and physical characteristics of the final material. The aim of this doctoral work is to understand the relations between cooling patterns during freezing and the structure at the macro and micro levels of the final freeze casted part. The current work comprises the development of a heat transfer model to efficiently and reliably predict the temperature evolution during freezing. In this way, it will be possible to recognize which are the process variables affecting the final pore morphology. The results of this work will improve the

fundamental knowledge of the process, serving as a tool to predict and control the microstructure obtained in the Freeze Casting process.

The problem definition and goals of this work are presented in chapter 1. A brief description of the main literature on freeze casting is presented in chapter 2. The development of a numerical model that calculates the temperature distribution within the experiment domain was carried out in chapter 3. In chapter 4, an alumina tile was produced by freeze casting process in order to test the freezing device, colloidal suspension characteristics and sintering temperature of the sample. Additionally, an analytical model was proposed for predicting the thermal conductivity of the material. Chapter 5 evaluates the effect of solid content and freezing temperature on pore morphology and evaluates how these variables affect the temperature distribution within the experiment domain. Chapter 6 compares the steady solution of the numerical model and the pore morphology obtained experimentally under different process parameters. Finally, conclusions and future work for the study are presented in chapter 7.

Products

As a result of this doctoral research the following products have been obtained:

Peer reviewed publications

Gil-Durán, S. & Ossa, E.A. (2016). Kaolin based ceramics obtained by Freeze casting process. Ingeniería y competitividad, 18(2), 133-140.

Gil-Durán, S. D. Arola, Ossa, E.A. (2020). Control of porosity in freeze casting. JOM – Springer, DOI 10.1007/s11837-019-03974-y.

Oral conference presentations

Gil-Durán, S. & Ossa, E.A. (2015). Obtención de cerámicos a base de caolín mediante el proceso de Freeze casting. VIII Congreso Internacional de Materiales.

Gil-Durán, S. & Ossa, E.A. (2016). Understanding freeze casting solidification process. TMS 2016 145th ANNUAL MEETING & EXHIBITION. Nashville, Tennessee.

Mesa-Toro, C. M; Gallego G; Ossa, E.A. Gil-Durán, S. (2017). Development of refractories by freeze casting processing. IMRMPT - International Meeting for Researchers in Materials and Plasma Technology

Mesa-Toro, C. M; Gallego G; Ossa, E.A. Gil-Durán, S (2018). Multifunctional ceramics for refractories applications. Congreso ALAFAR 2018.

Contents

List of tables

List of figures

Figure 4.3 X-ray computed tomography Density gray value at different sintering temperature as a function of thickness.

Figure 4.4 Changes of thermal conductivity as a function of lamellar fraction and total porosity of the sample.

Figure 5.1. Distinctive samples characteristics. a. bottom of the sample. b. transition zone c. Top of the sample. Sample prepared with 30% solid content frozen at 203K.

Figure 5.2. Lamellar zone length with respect to total sample length at different freezing rates and solid fractions. The error bars indicate standard deviation.

Figure 5.3 Temperature distribution as function of cooling temperature and solid content a. 203K, b. 143K, c. 93K 10% solid content d. 203K, e. 143K , f. 93K 30% solid content g. 203K , h. 143K, i. 93K 50% solid content.

Figure 5.4 Density of the lamellar zone at different freezing rates and solid content. The error bars indicates the standard deviation.

Figure 6.1. Schematic diagram showing the experimental setup and boundary conditions used in the finite element modeling. The points indicated in the slurry at 0.3L and 0.7L represent positions selected for analysis close to the axis of the slurry (C) and to the mold (M).

Figure 6.2. Freeze casted sample manufactured using the aluminum mold at cooling temperature of 203K. a) Micro-CT image; the scale bar represents 10 mm. b) Optical microscopy image showing the lamellar pore morphology; the scale bar represents 500 µm.

Figure 6.3 Micro CT images of the freeze casted samples manufactured using the aluminum mold at cooling temperatures of: a) 203K, b) 143K and c) 103K. Corresponding freeze casted samples manufactured using the rubber mold are shown for cooling temperatures of: d) 203K, e) 143K and f) 103K. The blue dashed lines indicate aligned porosity orientations. The scale bar in each figure represents 10 mm. Both aluminum and rubber mold dimensions were of 40 mm inner diameter, height 50 mm and 5 mm of wall thickness.

Figure 6.4 Measured variation of pore density (Pores/mm) as a function of freezing temperature for different positions within the freeze casted samples. a) Aluminum mold; b) Rubber mold.

Figure 6.5 Effect of mold geometry on temperature differences calculated using the FEA. a) mold thickness; b) mold internal diameter.

Figure 6.6 Effect of thermal variables on temperature differences as calculated using the FEA. a) freezing temperature; b) convective coefficient; c) thermal conductivity.

Figure 6.7 Calculated temperature differences with varying molds and freezing temperatures. Aluminum mold: a) 203K; b) 143K; c) 93K. Rubber mold: d) 203K; e) 143K; f) 93K.

Figure 6.8 Relation between temperature gradients and pore orientation for a) Aluminum mold with freezing temperature of 93K. b) Rubber mold with freezing temperature of 143K. The arrows indicate the direction of temperature gradient and a-axis of crystal growth. The scale bar represents 1mm.

CHAPTER 1 INTRODUCTION

Porosity plays a major role in controlling the behavior of any material. The Freeze Casting process allows obtaining synthetic materials with a control of the pores formed within the material (Deville, 2008; Gutierrez et al, 2008; Li et al., 2012; Gil-Durán & Ossa, 2016). The process consists of freezing a fluid, in which fine particles are suspended. Depending on the fluid, the crystals formed during freezing will have different shapes. When a crystal is formed, the frozen front moves the particles around them allowing particles to agglomerate around the crystal. The frozen samples have to be lyophilized in order to sublimate (transform the solid phase directly to a gas phase) the frozen solid phase. As a result, the lyophilized sample obtains a porous structure with a replica of the crystals' shape formed during freezing.

As Freeze Casting is a process where the pore characteristics are a result of the fluid solidification, the driver of the crystal nucleation and growth during freezing must be the temperature distribution within the medium. Although abundant literature is available about the Freeze Casting process, the fundamental aspects of ice nucleation and growth, which is the result of atomistic events driven by thermal fluctuations is far from complete (Shanmugam et al., 2016; Kristen L. S. & David C. D., 2018). Consequently, cooling patterns during freezing may result in a particular pore morphology and distribution within the final material. As of yet, there has not been a study that systematically analyses the relations between cooling patterns during freezing and physical characteristics like density and porosity of the final part. The aim of the current study is to test the hypothesis that the physical properties of the material obtained by the Freeze Casting process can be predicted by the cooling patterns during

freezing. It includes the development of a heat transfer model to efficiently and reliably predict the temperature evolution during freezing in order to better understand the fundamental aspects of ice nucleation and growth driven by the cooling patterns. This work will help establish the fundamental aspects of Freeze Casting that are affected by the temperature evolution during freezing. When properly understood, it will serve as a flexible tool to predict and control the obtained physical properties and it could lead to the development of novel synthetic materials for a wide range of applications such as bone substitute (Chen et al., 2020), solid oxide fuel cells (SOFC) (Chen et al, 2012; Lichtner et al, 2015; Xu & Wang, 2015; Arai & Faber., 2019), thermal insulation (Fukushima & Yoshizawa, 2014; Yang et al, 2015), gas cleaning (Kitaoka et al., 2004), catalysts supports (Pham-Huu et al., 1999), drug delivery systems (Szepes et al., 2007) and sound absorbing ceramic materials (Frank et al., 2011), among others (Hammel et al., 2014; Liu et al., 2016; Pagano et al., 2020).

The **general objective** of this work is to test the hypothesis that the morphological characteristics of the material obtained by the Freeze Casting process can be predicted by cooling patterns while freezing. It includes the development of a heat transfer model to efficiently and reliably predict the temperature evolution during freezing, in order to better understand of the fundamental aspects of ice nucleation and growth driven by the cooling patterns, so it will be clear how these patterns affect the morphological characteristics of the material.

Specific Aim 1: Test the hypothesis that the temperature distributions in the ceramic slurry when freezing depend on process variables (e.g.: mold material, dimensions, freezing rates, convection, etc). This will be accomplished by solving the heat equations in relation to boundary conditions in a domain representing the variables

of the process. The results of the heat transfer model will improve the process reliability by establishing recognition of the fundamental aspects of the temperature evolution during freezing.

Specific Aim 2: Test the hypothesis that the physical properties of materials obtained by freeze casting depend on setting specific experimental process variables, through the development of an experimental set up that allows controlling the variables of the Freeze Casting process. Aiming at being able to predict and control the solidification of the freezing liquid, through different process variables conditions.

Specific Aim 3: Test the hypothesis that there is a relationship between the morphological characteristics achieved in the sintered part and the temperature distribution within the Freeze casting process, through an analysis of cooling patterns while freezing and the density and porosity of the obtained samples under different process variables conditions. In order to better understand the fundamental aspects of the physical properties driven by the cooling patterns.

CHAPTER 2 LITERATURE REVIEW

The following chapter summarizes the four basics steps of the Freeze casting process, paying special attention to the process variables that end up affecting the morphology of the material, in addition to the fundamental aspects of water ice crystal growth and the mechanisms controlling it.

2.1 Freeze Casting

Materials are often divided into distinct classes. The primary classes of solid materials are ceramics, metals, polymers and composite materials. Ceramic materials have a combination of covalent, ionic and sometimes metallic bonding. The majority of ceramics are a compound of metal or metalloids and non-metals. They have specific properties associated with them such as brittleness, poor thermal conductivity, high compressive strength and chemical insensitivity. However, there are also a few exceptions to these general characteristics of ceramics. Ceramic materials can be classified in different ways based on chemical composition, applications, and mechanical properties, among others. One that is commonly found in text books is to classify them into traditional and advanced ceramics. Traditional ceramics are usually based on clay and silica and their application includes high volume items like bricks, white ware and kitchen ware. Alternatively, advanced ceramics exhibit superior properties for demanding applications such as structural ceramics, electronic ceramics, and bio-ceramics. One of the main differences between these two groups is in terms of the raw materials and the forming processes (Carter & Norton, 2013).

The three most important facts in what determines the mechanical properties of a material are the material used for the part, the morphology of the pore and the relative density (Ulrike et al, 2010). Scientists have explored diverse manufacturing methods aiming at obtaining synthetic materials with controlled porosity (Sellinger, et al, 1998; Tang et al, 2003, Seitz et al, 2005; Fu e al., 2011; Li et al,. 2012;). Between them, Freeze casting is a relatively new technique that allows a control of the pore size and shape formed within the material based on setting specific process variables (Deville, 2008; Gutierrez et al, 2008; Qian & Zhang, 2011; Li et al., 2012). The porosity of freeze casting materials most frequently obtained can be qualitatively described as being lamellar, dendritic, cellular, honey comb and/or columnar. The flexibility of the process is on the one hand an advantage but on the other it adds significant complexity when attempting to understand the principles that govern porosity-process relationships. There have been initiatives using freeze casting to produce solid oxide fuel cells (SOFC) (Chen et al, 2012; Lichtner et al, 2015; Xu & Wang, 2015), thermal insulation (Fukushima & Yoshizawa, 2014; Yang et al, 2015), gas cleaning (Kitaoka et al., 2004), catalysts supports (Pham-Huu et al., 1999), drug delivery systems (Szepes et al., 2007), sound absorbing ceramic materials (Frank et al., 2011), bioinspired materials for bone replacement (Deville et al, 2006), among others (Hammel et al., 2014; Liu et al., 2016).

2.2 Process description

In general, freeze casting offers a wonderful opportunity to create synthetic materials that could lead to the development of novel structures for a wide range of

applications. As follows, the freeze casting process is illustrated and consists of four basic steps as schematically shown in figure 2.1.

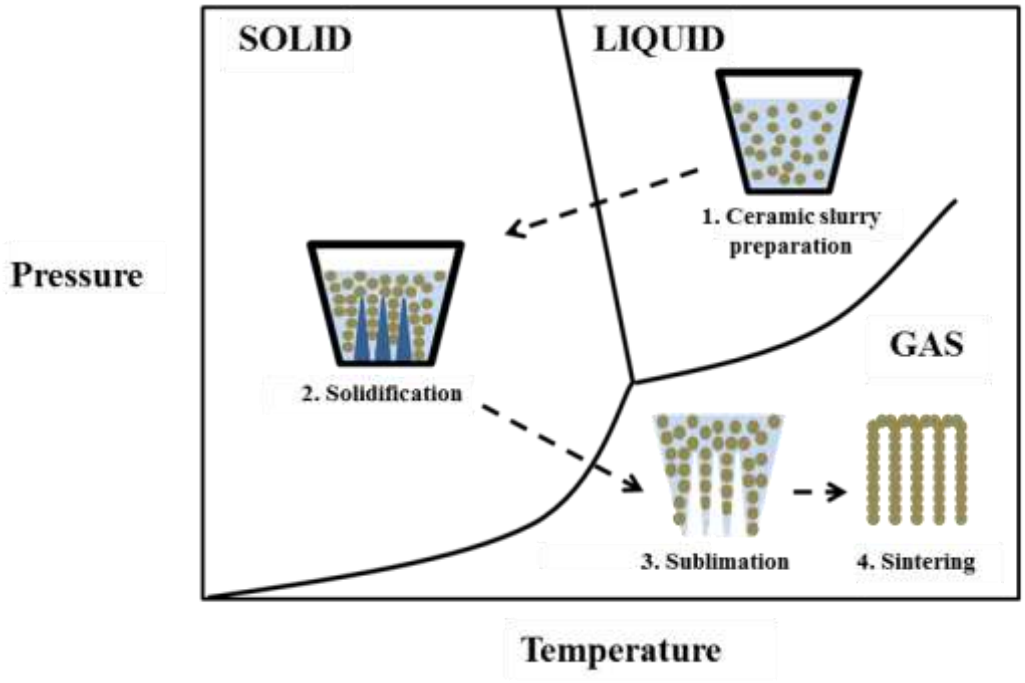

Figure 2.1. *The freeze casting process consists of four basic steps. 1. Ceramic slurry preparation; 2. Freezing the ceramic-solvent system; 3. Sublimation of the frozen solvent; and 4. Sintering of the ceramic.*

2.2.1 Ceramic Slurry preparation

In general, for freeze-casted materials, pore morphology is mainly determined based on the slurry preparation. The slurry consists of colloidal particles that are suspended in a medium (fluid), the most common particles used are ceramics, however, metallic and polymeric can also be employed (Deville, 2008). The slurry prepared for freeze casting can be produced using different types of medium. For instance, the most commonly used are water, camphene and tert-Butyl alcohol based (Naviroj et al., 2017),

each of them producing different pore structures which leads to different characteristics of the resultant material. Figure 2.2 shows different pore morphologies obtained using different types of mediums. Figure 2.2a and 2.2b show how additives are also added to the fluid to tailor pore structures by manipulating the crystalline structure of the solidified fluid or modified particle redistribution (Kristen & David, 2018). Figure 2.2c shows the pore morphology using cyclohexane as a medium. As a result the flexibility of the process is one of the main benefits of the freeze casting process.

The concentration of the particles within the slurry has an effect on the final part. With increasing particles concentration, the material will be less porous (Deville & Bernard-Granger, 2010). It follows a linear relationship between porosity and initial solid content of the slurry (Tang et al., 2013; Flauder et al., 2014). Another important parameter is the particle size, as it gets smaller more detailed structures can be copied (Deville, 2008). In the event that different particle sizes are being used, it is important to study their distribution in ceramic slurries to ensure homogeneity of the resulting part. As ceramic particles generally include cations (+charged) and anions (-charged), it is also important to know the chemistry interactions that occur within the slurry. If it is not properly prepared, the slurry can become unstable producing sedimentation, creaming and flocculation, among other unwanted phenomenon that affect the final structure. Colloidal interaction governs whether the particles aggregate or remain separated. Attractive forces tend to destabilize colloids, whereas repulsive forces generally impart stability (Carter & Norton, 2013). The dispersion of the particles within the medium can be modified by changing the ionic strength or altering the pH, also called electrostatic stabilization. Steric forces are an alternative to modify the stability of the slurry. Here, organic molecules including polymers, copolymers and dispersants are introduced to the

medium to anchor the particles surface via absorption. Electrosteric force is the method most commonly used to obtain stabilized slurry (Cesarano et al, 1988). Polyelectrolyte species cause both electrostatic and steric stabilization simultaneously. Chemical and physical properties of the particle's surface and medium can be affected by adsorption of polyelectrolytes (Biggs & Healy, 1994). Higher adsorbed concentration favours stability, whereas low adsorbed concentration promotes flocculation. Adsorbing can be modified by changing the pH of the medium. (Lewis, 2000).

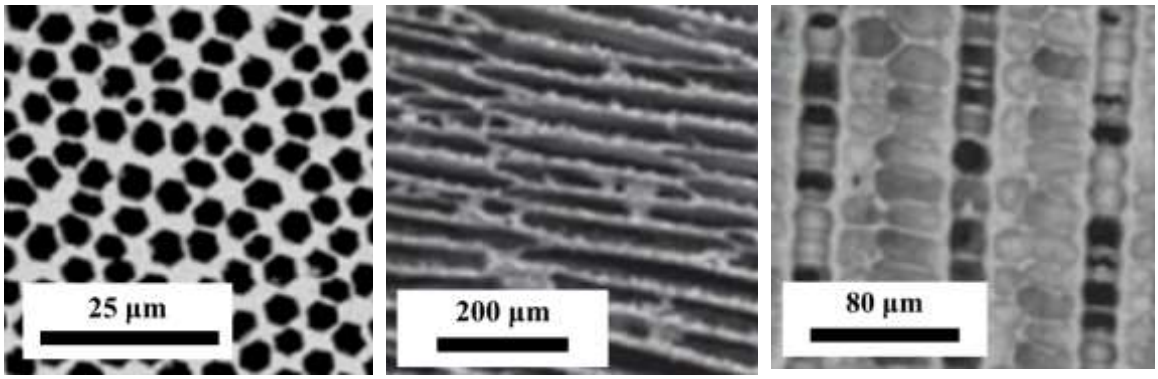

a. b. c.

Figure 2.2. *Pore morphologies obtained using freeze casting.* ***a.*** *Effect of the addition of zirconium acetate complex to an aqueous suspension (Souza et al., 2014);* ***b.*** *Effect of the addition of isopropyl alcohol to an aqueous suspension (Onna et al., 2015); and* ***c.*** *using cyclohexane as a medium (Sobolev, S. L., 2012).*

The choice of the medium and additives largely determines the resulting pore morphology. Water based suspensions are so far the most studied, since there is a wide range of porosity structures that can be achieved. The predominant pore structure obtained when using water based slurries is lamellar, which are plate like walls. They

can have a morphological transition from lamellar to dendritic to cellular by changing suspension characteristics through additives (Sofie & Dogan., 2001; Pekor et al., 2008; Pekor & Nettleship., 2014,). Binders, which are used to enhance the strength of the freeze-cast material in green state (without sintering), have been used by Peko et al., (2010) to induce morphological transition from lamellar to dendritic via increasing the amount of binder (polyvinyl alcohol, PVA). Similar results have been found for freeze-cast based on yttria-stabilized zirconia (Zuo et al., 2008) and hydroxyapatite (Zuo et al., 2010). Figure 2.3 shows a couple of microstructures obtained with water as a medium and the effect of the binder. Figure 2.3a shows the resulting microstructure with no binder and figure 2.3b with 20 wt%. of the dry powder. Furthermore, gelatin was employed as a binder for tungsten disulfide powder (Wu et al., 2017; Wu et al., 2018) and hydroxyapatite (HAP) (Qian et al., 2009). Conclusions obtained indicate that as it is increased the amount of gelatin the pore morphology was changed from lamellar to dendritic to cellular. Sucrosse has also been studied to trigger dendritic to cellular transitions (Munch et al., 2009).

When water and simple alcohols are mixed to create a binary medium, the pore interconnectivity and aspect ratio can be tailored based on the employed alcohol concentration (Naleway et al., 2015; Jing et al., 2014). In further studies, it has been proven that the addition of zirconium acetate to an aqueous medium, even with different types of particles such as Al_2O_3 (Bouville et al., 2014), SiC (Deville et al., 2011), and zircona (Zou et al., 2017), can lead to honeycomb structures (Deville et al., 2011). All these transitions are attributed to the increase in suspension viscosity (Liu et al., 2015) and reduction in flocculation (Delattre et al., 2013; Kumaraswamy et al., 2016). Glycerol is commonly employed as a medium allowing to obtain interconnectedness

(Liu & Button, 2013), modify pore width, and at higher solid fractions allowed to obtain cellular microstructures (Sofie., 2007) amongst others (Okaji et al., 2013; Chu et al., 2015). Thus, it is of crucial importance to know the slurry chemistry when attempting to control the pore characteristics.

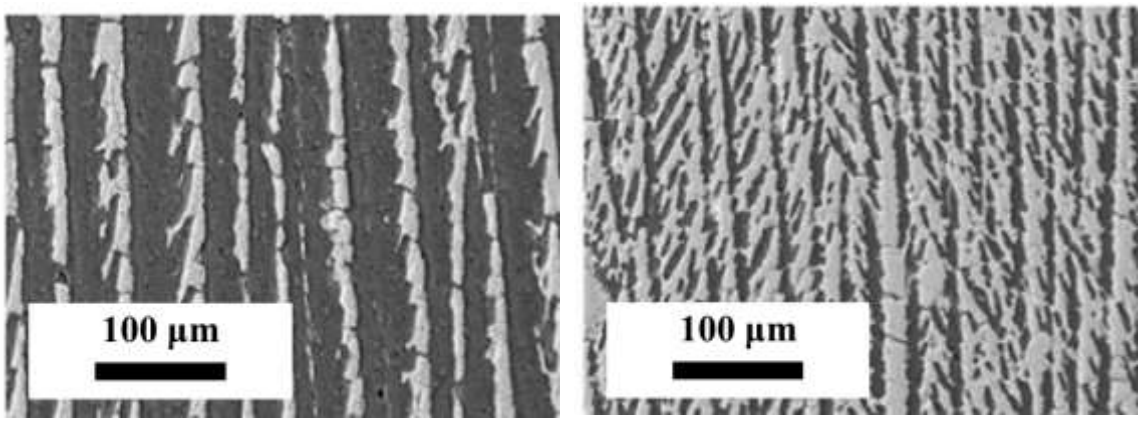

a. b.

Figure 2.3. *Pore morphology with aqueous suspensions and the effect of binder polyvinyl alcohol (PVA). a. no binder; b. 20 wt%. (Peko et al., 2010).*

2.2.2 Freezing the ceramic-slurry

After the ceramic slurry is properly prepared, it is frozen. It is important to bear in mind that depending on the medium and additives used in the slurry preparation, the crystals formed during freezing will have different characteristics. However, during freezing particular process variables that affect the pore morphology are: the freezing direction (Deville, 2008), freezing rate (Wegst et al, 2010; Gil-Durán & Ossa, 2016), pressure while freezing (Eisenberg & Kauzmann, 2005) and magnetic field (Porter et al., 2012).

Freeze casting can be classified as anisotropic or isotropic freezing, being the anisotropic freezing the one most studied. Isotropic freezing is used when nonaligned porosity is required (Yang et al., 2005), porosity obtained range from closed equiaxed cells (Mallick & Winnett., 2012) to open reticular networks (Blindow et al., 2009) with structures being nearly isotropic. On the other hand, when aligned porosity is required the technique use to freeze the sample is anisotropic (Gil-Duran et al., 2020). In anisotropic freezing, the solidification typically takes place in one direction which is promoted by how the slurry is frozen, typically the freezing of the sample is promoted vertically from the bottom to the top of the sample. However, radial freezing has also been used (Moon et al., 2003; Bai et al., 2015; Seuba et al., 2017). Thus, the way the sample is frozen will lead to obtain microstructures with different pore characteristics.

In general, during freezing it is essential to be able to control the freezing rate as it can have an impact on the final structure obtained, affecting the pore characteristics and mechanical properties of the material obtained (Ulrike et al, 2010). When a crystal is formed the frozen front moves the particles around them, allowing particles to agglomerate around the crystal. If the solidification rate is very high the particles are not push ahead and they end up engulfed leading to unaligned porosity. As Freeze Casting is a process where the pore characteristics are the result of fluid solidification, the driver of the pore morphology must be the temperature distribution within the medium. Consequently, cooling patterns during freezing may result in a particular pore morphology and distribution within the final material as can be inferred by comparing the images in figure 2.4. So far, there has not been a study that systematically analyses the relations between cooling patterns during freezing and physical characteristics, like

density and porosity of the final part. This topic will be studied in the following chapters.

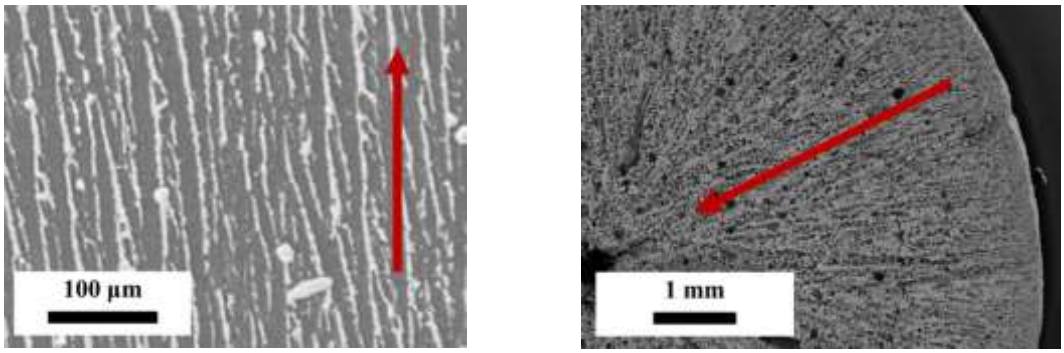

a. b.

Figure 2.4. *Pore morphology freezing direction a. (Zhang et al., 2017) b. (Macchettaa et al., 2009). The arrows indicate the freezing directions.*

In recent years much work has been done in observing how experimental aspects of freeze casting process affects the material morphology, yet, little attention has been paid to the phase transition from water to ice crystal driven by cooling patterns. A knowledge of how water crystals grow is a potentially important tool to be able to predict the material morphology obtained. During the phase transition of water from liquid to ice, the disordered liquid molecules are organized via hydrogen bonding (Hobbs., 2010). The solidification process can be divided into two steps, nucleation and crystal growth, both having an impact in the crystal formed.

During nucleation, water molecules are organized to form the first solid that then will grow forming the crystals. The temperature at which this occurs is called nucleation temperature and ranges from 273K to 233K for water. In between these values, small clusters of molecules are ordered but with no long range order. This is also

called primary nucleation (Matsumoto et al., 2002; Ayel et al., 2006) which is a stochastic process that cannot be completely controlled, however it has been shown by Wilson et al. (2003) that with the addition of nucleation agents the nucleation process can be somehow tuned by narrowing the ranges of temperatures at which nucleation occurs. Once it has occurred, any new nuclei formed undergoes a process called secondary nucleation which leads to the development of new crystals, (Myerson., 2002; Flemings., 1974). After the initial nucleation occurs, the remaining liquid is frozen by ice crystal growth (Rey & May., 2004).

2.2.3 Sublimation

Once the freezing has been completed, the samples have to be lyophilized in order to sublimate the frozen liquid phase. Sublimation is the transformation of a solid phase directly to the gas phase. As a result the lyophilized sample has a porous structure with a replica of the crystal's shape formed during freezing. The samples after sublimation are also said to be in a green state, where it can hold the form and shape. Nevertheless it does not stand mechanical loads. The sublimation process takes place in a camera with low temperature and pressure. The values are particular to each solvent (Deville, 2008), and to the best of my knowledge there has not been studies that report effects on the pore morphology by changing lyophilisation process variables.

2.2.4 Sintering

As a final step, sintering of ceramics is performed in a furnace. In freeze casted ceramics the samples have to be sintered after sublimation. High temperatures are needed because of the low self-diffusion coefficient in the solid state. With temperature the particles become a denser structure joined by grain boundaries. Depending on the

sintering temperature the freeze casted material can become a denser structure affecting pore morphology (Plucknett et al., 2008). This process starts with individual particles making a point contact, then, due to the high temperature they begin to form a neck, and possibly to entirely form a new, bigger grain from various smaller grains. High temperature is also needed for phase transformation involving crystallization. Controlling the temperature is required to ensure that the crystalline phase is formed and the desired density is reached (Carter & Norton, 2013). Therefore, it is important to pay attention to conditions in the sintering process with the aim of optimizing the physical and mechanical properties of the final ceramic component (Liu., 2011).

2.3 Freeze casted ceramics applications

With the development of new technologies, materials with multifunctional characteristics are required (Scotti & Dunand., 2018; Algharaibeh et al., 2019). The development of new unconventional processing routes that allows to methodologically design and control microstructures it's of extreme importance. There have been different processing routes already studied, such as partial sintering, replica and sacrificial template, direct foaming and others. (Studart et al., 2006). The selection of the process depends essentially on the desire material characteristic.

As it has been shown through this chapter, several different pore morphologies can be obtained using freeze casting, making it attractive because the easy control of porosity. The main interest of this thesis is on controlling porosity using finite element analysis to obtain materials with controlled structures that can have different properties in different regions. These type of materials are called functionally graded materials

(FGM) and are designed for a specific performance or function. FGMs are fabricated to obtain materials with gradual changes in macroscopic properties, where pore morphology and distribution are controlled (Naebe & Shirvanimoghaddam., 2016). The application of such materials includes uses where different hardness, specific heat and mass density are required, for example, furnace liners, prosthesis with biocompatibility, body armor, piezo electric actuators, electromagnetic sensors and others (Pagano et al., 2020). Thus, the following chapters are aimed at understanding how finite element analysis FEA can be used to tailor pore morphologies and structural properties in specific directions, an approach combining numerical and experimental analysis to physically understand how to obtain tailored properties.

CHAPTER 3 NUMERICAL SIMULATION. UNDERSTANDING FREEZE CASTING SOLIDIFICATION PROCESS

The aim of this chapter is to develop a numerical model which calculates the temperature distribution within the experimental domain by solving the heat equation with given boundary conditions. The simulations were validated by using an analytical model.

3.1Introduction

The freeze casting process can be used to tune the pore morphology characteristics by setting specific process variables as seen in chapter 2. The use of numerical simulations to predict the pore morphologies of freeze casted materials have not received much attention and it is a potential tool to control the development of the pore network to fabricate reproducible materials.

The importance of the freezing process in the freeze casting has been recognized in recent years. It takes place in a freezing apparatus that is designed to control the freezing process. There have been different setups used for freeze casting as shown in figure 3.1. Liu., (2011) utilized an experimental setup employing liquid nitrogen as a freezing media contained in a liquid nitrogen dewar. A different way of freezing is using a cold finger where the temperature can be monitored and manipulated by combining a cold bath with ring heaters. Preiss et al (2012) used a more elaborated device with a double sided cooling apparatus in which the temperature was controlled

with band heaters and thermocouples in both sides of the slurry. The freezing apparatus is the most essential elements used in the freeze casting process since the crystal nucleation and growth is controlled during freezing (Deville et al., 2007; Waschkies, et al., 2011).

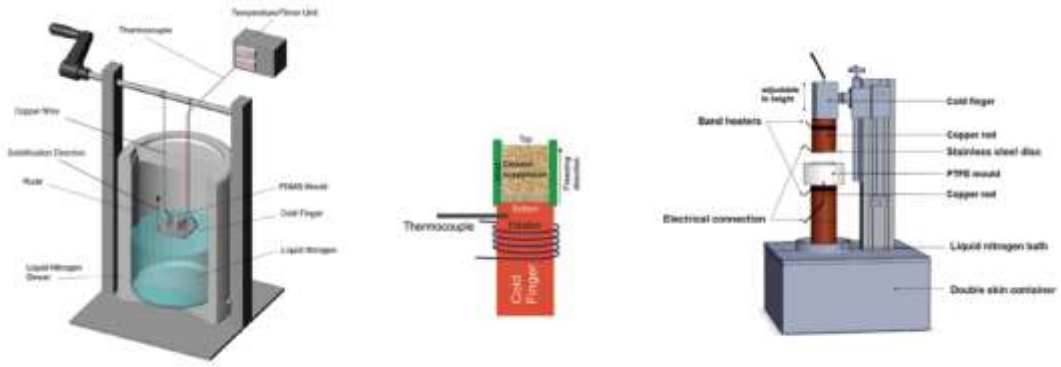

Figure 3.1. *Experimental apparatus for freeze casting by Liu. (2011); Waschkies et al. (2011) and Ping et al. (2014).*

The development of the crystal is governed by three physical processes: mass diffusion, flow rate of latent heat away from the liquid/crystal interface, and the specifics of the particle attachments at the liquid/crystal interface (Knrpnrnrcr, R. J., 1975). In the matter of water ice crystal, the flow rate of latent heat away from the surface plays by far the most important role, consequently, the experimental set up has to be analyzed focusing on the thermal aspects of the model (Pawelec et al., 2014). Studies that use FEA to analyze freeze casting includes the effects of mold design with varying contact areas within the heat sink to modify pore structure (Pawelec et al., 2015). Highly porous SiC ceramics have also been obtained by using several freezing

conditions combined with finite element analysis (Wang et al., 2019). The use of numerical simulations to predict the structures and morphologies of freeze casted materials have been also applied to produce porous scaffolds from collagen (Husmann et al., 2015) and chitosan-alginate scaffolds (Rouhollahi et al., 2019).

Thus, computer simulation is a promising route for creating complex designs with ceramic materials. The aim of this chapter is to develop a numerical model which calculates the temperature distribution within the experimental domain by solving the heat equation with given boundary conditions. The simulations were validated by using an analytical model. The numerical simulations will be used to predict the pore morphologies of freeze casted materials in the following chapter.

3.2 Constitutive equations and modeling

In the current thesis the experiment setup used to freeze the samples consist of a manually operated elevator and liquid nitrogen as a freezing media contained in a liquid nitrogen dewar. The elevator consists of a thin plate made of aluminum that is connected with the elevator. A wide range of freezing temperatures can be obtained by adjusting the distance between elevator and the surface of the liquid nitrogen. On top of the aluminum plate it will be positioned a cylindrical mold that contain the ceramic slurry.

The heat transfer problem for simulating such cooling process is illustrated in Figure 3.2. The experiment setup previously described can be simplified to an axisymmetric problem with three domains corresponding to: i) the cooling plate; ii) the

mold material; and iii) the ceramic slurry. Each domain having its own thermal properties. The boundary conditions (BC) of the model were defined as (Lewis et al., 1996): Dirichlet boundary conditions, referring to a situation where the temperature at any surface is controlled directly. In our domain, the bottom of the experiment which is in direct contact with the cooling elements were set to maintain a fixed constant temperature with this BC. On the other hand, Neumann boundary conditions equal to zero models a situation where the rate of flow of heat is controlled. In our experiments, this condition was applied to the axisymmetric axis since the heat cannot enter or leave through that boundary. Finally, Robin boundary conditions were applied as a convective boundary condition. In our experiment it was used to represent the movement of the air around the experiment.

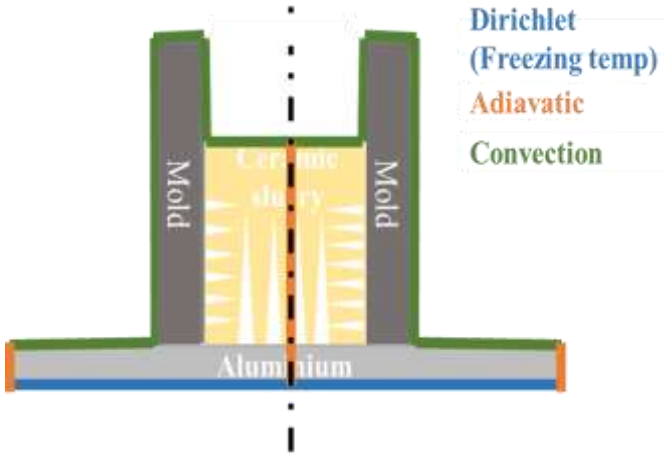

Figure 3.2. *Domain and boundary conditions of the heat transfer model.*

The heat equation, which is a parabolic partial differential equation, can be written as:

$$\frac{\partial \mathrm{T}}{\partial \mathrm{t}} - \alpha \nabla^2 T = 0 \,, \quad \textbf{(3.1)}$$

where α is the thermal diffusivity defined as:

$$\alpha = \frac{k}{C_p \rho} \ . \quad \textbf{(3.2)}$$

Being *k* the thermal conductivity, *Cp* the specific heat capacity and ρ the mass density of the material.

From the heat equation (3.1), $\nabla^2 T$ can be defined in cylindrical coordinates as an axisymmetric problem as:

$$\nabla^2 T = \frac{1}{r}\frac{\partial}{\partial r}\left(r\frac{\partial T}{\partial r}\right) + \frac{1}{r^2}\frac{\partial^2 T}{\partial \emptyset^2} + \frac{\partial^2 T}{\partial z^2} \ . \qquad \textbf{(3.3)}$$

By means of symmetry in the problem, $\nabla^2 T$ loses the dependence with respect to $\emptyset$. Then:

$$\nabla^2 T = \left(\frac{1}{r}\frac{\partial}{\partial r}\left(r\frac{\partial T}{\partial r}\right) + \frac{\partial^2 T}{\partial z^2}\right). \qquad \textbf{(3.4)}$$

Now, the heat equation can be written as:

$$\frac{\partial \mathrm{T}}{\partial \mathrm{t}} - \alpha\left(\left(\frac{1}{r}\frac{\partial}{\partial r}\left(r\frac{\partial T}{\partial r}\right) + \frac{\partial^2 T}{\partial z^2}\right)\right) = 0. \qquad \textbf{(3.5)}$$

To simplify the heat equation, by multiplying by r we obtain:

$$r\frac{\partial \mathrm{T}}{\partial \mathrm{t}} - \alpha\frac{\partial}{\partial r}\left(r\frac{\partial T}{\partial r}\right) + \alpha\frac{\partial^2 T}{\partial z^2} = 0. \qquad \textbf{(3.6)}$$

The second term of the equation can be rewritten as:

$$r\frac{\partial^2 T}{\partial z^2} = \frac{\partial}{\partial z}\left(r\frac{\partial T}{\partial z}\right). \qquad \textbf{(3.7)}$$

Thus the heat equation becomes:

$$r\frac{\partial \mathrm{T}}{\partial \mathrm{t}} - \alpha\frac{\partial}{\partial r}\left(r\frac{\partial T}{\partial r}\right) + \alpha\frac{\partial}{\partial z}\left(r\frac{\partial T}{\partial z}\right) = 0 \ . \textbf{(3.8)}$$

If $\nabla_{r,z}$ is defined as:

$$\nabla_{r,z} = \begin{bmatrix} \frac{\partial}{\partial r} \\ \frac{\partial}{\partial z} \end{bmatrix}, \qquad \textbf{(3.9)}$$

the heat equation can be expressed by means of:

$$\boxed{r\frac{\partial \mathrm{T}}{\partial \mathrm{t}} - \alpha\nabla_{r,z}(\mathrm{r}\nabla_{r,z}\mathrm{T}) = 0} \quad \textbf{(3.10)}$$

Boundary conditions due to the convective process are listed below:

$$\boxed{-\alpha\frac{\partial \mathrm{T}}{\partial \mathrm{n}} = h_c\left(T - T_{inf}\right)} \quad \textbf{(3.11)}$$

Where h_c is the convective coefficient and T_{inf} the temperature surrounding the domain. Natural convection in air h_c ranges in values from 3 to 20 [W/m^2-K] (Oosthuizen P. H & Naylor D., 1999). Here it was assumed to have a value of 10. Then, the weak form of the heat equation takes the form:

$$\boxed{\int_\Omega w\, r\, \frac{\partial \mathrm{T}}{\partial \mathrm{t}}\, dV + \alpha\int_\Omega \langle \nabla_{r,z} w, r\nabla_{r,z}\mathrm{T}\rangle\, dV + \int_\Gamma w\, r\, h_c\left(T - T_{inf}\right) = 0} \quad \textbf{(3.12)}$$

A theta (θ) scheme in the time is used, to be able to solve the implicit, explicit model. The time dependent term is:

$$\frac{\partial \mathrm{T}}{\partial \mathrm{t}} = \frac{T_{i+1} - T_i}{\Delta t}, \qquad \textbf{(3.13)}$$

where T_{i+1} and T_i are the unknown and known temperature respectively. Therefore, the weak form is given as:

$$\int_{\Omega} w\, r\, \frac{T_{i+1}-T_i}{\Delta t}\, dV + \theta\left(\alpha \int_{\Omega} \langle \nabla_{r,z} w, r \nabla_{r,z} T_{i+1} \rangle\, dV\right) + (1 -$$

$$\theta)\left(\alpha \int_{\Omega} \langle \nabla_{r,z} w, r \nabla_{r,z} T_i \rangle\, dV\right) + \int_{\Gamma} w\, r\, h_c\left(T - T_{inf}\right) dV = 0 \qquad \textbf{(3.14)}$$

In this case:

- $\emptyset = 1$ implicit
- $\emptyset = 0$ explicit
- $\emptyset = 0.5$ Crack Nicholson

Freefem++ software was used to solve this problem. Comparison of the relative error within uniform and adapt mesh with P1 and P2 element behavior was performed to analyze convergence of the solution. The relative error was defined as:

$$Relative\ error = \int_{\Omega} (T(t_i) - T(t_{i-1}))^2\ . \qquad \textbf{(3.15)}$$

3.3 Results

Comparison of the relative error using uniform and adapt elements with P1 and P2 behavior while increasing the size of the mesh is illustrated in Figure 3.3. As expected in uniform and adapt elements, the finer the mesh the better and more accurate approximation to the solution is achieved. Additionally, in both cases the P2 element behavior, which uses a higher order polynomial than P1, approximates quicker to the solution. In the current study it was used uniform mesh with P2 behavior to obtain the solution.

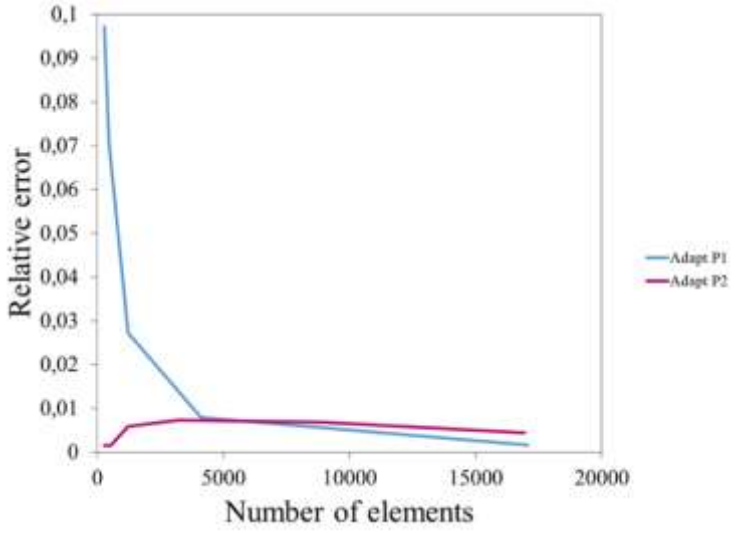

a.

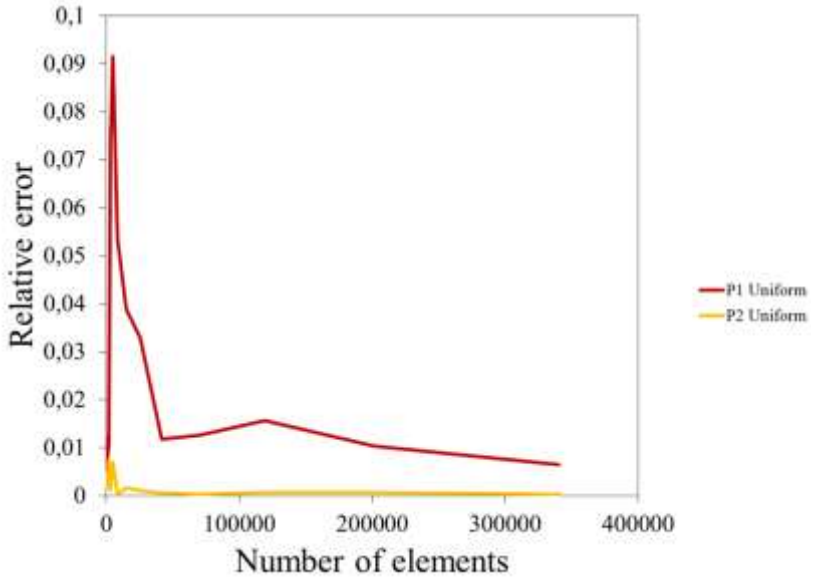

b.

Figure 3.3 *Comparison of the relative error using uniform and adapt elements with P1 and P2 behavior while increasing the size of the mesh. a) Adapt mesh; b) Uniform mesh*

In order to conclude if the Freefem++ model is a good approximation of a real solution, a comparison between a known analytical solution and the model will be performed. The procedure to calculate the analytical solution is showed below. First, the heat flow through the system is the same, then:

$$\left(k\frac{\Delta T}{L}\right)_{Cs} = \left(k\frac{\Delta T}{L}\right)_{Al} \quad \textbf{(3.16)}$$

Where L is the thickness of heat flow, k the thermal conductivity and ΔT the temperature change. After applying conservation of energy, the following is obtained:

$$673 - 373 = \Delta T_{cs} - \Delta T_{Al} \quad \textbf{(3.17)}$$

Solving the two-system equation, it was found:

$$\Delta T_{Cs} = 299 \quad \textbf{(3.18)}$$

Such result indicates that the temperature at the bottom of the ceramic slurry is reduced 299 degrees from the initial 673K. Then, the remaining temperature at the bottom of the ceramic slurry was 373K. Figure 3.4 shows the results of the analytical case using the software Freefem ++. According to the model the temperature at such point is 373.24 °C, which is in agreement with the analytical results, being the model a good approximation of the analytical solution.

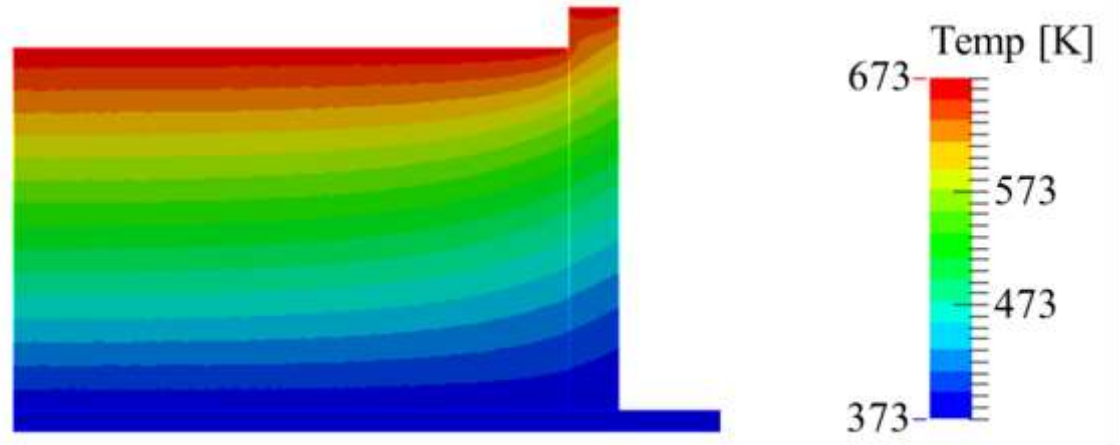

Figure 3.4. *Freefem++ result of the analytical case.*

The temperature evolution within the experiment is a time dependent process and the final gradient direction was obtained in short periods of time, obtaining the same results if the analysis was carried out after the steady state was reached. Therefore, after analysis of the final effect of the transient time dependent part of the process on the pore formation and orientations, it was found that there were no considerable effects.

3.4 Conclusions

In freeze casting process the cooling patterns observed during cooling can be predicted using a Finite Element Analysis model. The most common experimental setup that consists of a cylindrical mold can be successfully simplified to a 2D axisymmetric problem and solved obtaining an accurate solution. The Freefem ++ implementation served as a tool to establish the bases to start experimenting with freeze casting to be able to understand how process variables affect them in order to relate the cooling patterns to the desired microstructure of the final part.

CHAPTER 4 MODEL FOR PREDICTING THE THERMAL CONDUCTIVITY OF AN ALUMINA TILE PRODUCED BY FREEZE CASTING PROCESS

In this chapter an alumina tile was produced by freeze casting process in order to test the colloidal suspension characteristics, freezing device and sintering temperature of the sample. Additionally, an analytical model was proposed for predicting the thermal conductivity of the material taking into account pore characteristics.

4.1 Introduction

The Freeze casting process allows materials to be obtained with controlled microstructure as shown in chapter 2. Pagano et al., 2020 has proposed that one of the potential applications of freeze casting materials are furnace liners since it can reduce energy consumption with the maximum possible efficiency reducing CO_2 global emissions.

Refractory materials can be classified based on chemical composition and method of manufacture amongst others (Sadik et al., 2014). One that is often accepted is to classify refractories by the amount of porosity (Ishizaki et al., 2013). Refractories are mostly used in the industry due to their wide range of application and low cost. Initiatives of using Freeze Casting for refractories application have been encourage by Li & Li., (2012), they proposed the use of freeze casting to obtain porous Y_2SiO_5

ceramics. They observed that by decreasing the solid content from 20% to 10% leads to decreasing the compressive strength and thermal conductivity. Zhang et al., (2016) proposed a novel method to prepare silica aerogel/porous Y_2SiO_5 composites using freeze casting with the potential application as a high-temperature thermal insulation material. They concluded that the thermal conductivity decreases and the compressive strength increases remarkably while impregnating porous Y_2SiO_5 with silica aerogel. Similarly, Hautcoeur et al., (2016) used freeze casting to prepare ceramic/metal composites by aluminum alloy infiltration. Thermal conductivities were determined for zirconia/metal composites, with an average of 80 W m^{-1} K^{-1} and 13 W m^{-1} K^{-1} parallel and perpendicular to the freezing direction, respectively. Finally, Fukushima & Yoshizawa (2016) fabricated Mullite thermal insulators with high porosities of up to 91-vol% using a gelation freezing method. The thermal conductivity of the obtained thermal insulators ranged from 0.23 to 0.38 W m^{-1} K^{-1} at room temperature.

So far, the results obtained using freeze casting are promising for preparing ceramic thermal insulation materials. In such perspective, the aim of this chapter is to fabricate alumina tiles produced by freeze casting process, while evaluating the colloidal suspension characteristics, freezing device and sintering temperature of the sample. Additionally, an analytical model was proposed for predicting the thermal conductivity of the material taking into account pore characteristics.

4.2 Materials and methods

The ceramic slurry consists of an aqueous medium and ceramic particles. The medium used will be distilled water. Alumina powder as a ceramic material (30% solid content) and organic defloculant (polyvinylalcohol, 1.4 wt % of the alumina powder, 341584 ALDRICH Poly (vinyl alcohol), Mw 89,000-98,000), working as a defloculant and binder, increasing the strength of the green part (Launey et al., 2009). The zeta potential of the alumina slurry will be measured as a function of pH. The pH of the samples will be adjusted to different values from 2 up to 12. Zeta potential measurements will be carried out using Malvern Zetasize at room temperature (293K).

The freezing apparatus is one of the most important elements used in the freeze casting process (Deville et al, 2007; Waschkies, et al, 2011). The one employed in the current study was described in chapter 3. The sample was frozen at 203K in rubber molds of 50 mm x 50 mm. The frozen part was then freezed dried for 12 hours to allow the ice to sublimate (Preiss et al., 2012) (VirTis BenchTop 4K, 16 mTorr at 193K). Finally, sintering is performed in a convective furnace (Nabertherm LT 15/13/P330) at three different temperatures 1573K, 1673K and 1773K to observe how it affects the densification of the samples.

To achieve differentiation between specific physical properties at the macro and micro levels pore morphology and distribution within the samples was studied using optical microscopy (Zeiss Discovery.V8) on reflection mode. Sectioning by half the samples was performed to compare the effects of varying process parameters on pore morphology. X-ray computed tomography (CT), Cone Beam CT (Galileos, Sirona, Germany) 85 kV, 35 mA, 14.5 s, was employed to assess changes in density within the sample at the micro levels. Galaxis Galileos Viewer was used to assess the average grey value in a circular area of $r = 1\ mm$ to assess variations in density. Four measurements

of density were taken, each distributed equidistant from the bottom to the top of the sample. The bottom of the sample is where the freezing starts.

4.3 Results and discussion

The zeta potential characterizes the surface properties of the alumina particles in suspension. The magnitude of this parameter is often used as a measure of the strength of the repulsive interactions between particles. The dispersion of the particles within the medium are modified by changing the ionic strength or altering the pH as can be observed in figure 6.1. Polyelectrolyte species cause both electrostatic and steric stabilization simultaneously. In figure 4.1, between the pH ranges of 2–12, the zeta potential is positive at pH 2 and negative at pH 4, 6, 8, 10, 12. Chemical and physical properties of the particle's surface and medium are affected by adsorption of polyelectrolytes (Biggs & Healy, 1994). Higher adsorbed concentration favors stability, whereas low adsorbed concentration promotes flocculation. Adsorbing can be modified by changing the pH of the medium (Lewis, 2000). The isoelectric point, where the slurry is unstable, is located at pH ~ 2.5. Hence, as in this study it is desired to have particles in suspension, the alumina slurry will be left at its inner pH 6,0. Electrosteric stabilization is the method used to obtain an stabilized slurry (Cesarano et al, 1988).

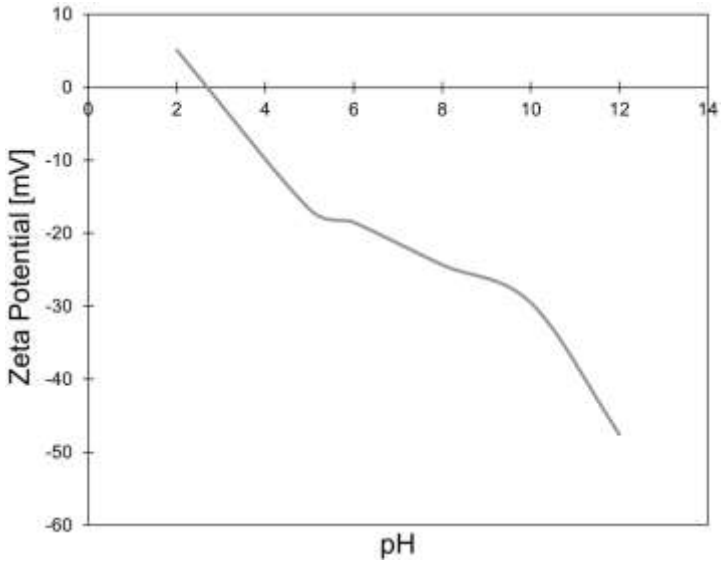

Figure 4.1 *Z-potential as a function on pH.*

Optical microscopy of the freeze casted samples show that the samples displayed three well-defined zones, each having different pore morphology, as shown in figure 4.2. At the top of the sample, figure 4.2a, appear well-defined lamellar macropores that get wider in the direction of the upper region. The pores are aligned with a branch-like structure. Lamellar macro-pores are the consequence of slower freezing front at the top of the sample resulting in a homogeneous ice nucleation (Schoof et al., 2001). Just directly below the top zone, there is a transition where the aligned pores begin to be formed from cellular to lamellar structures (Deville et al., 2006). The bottom of the sample, which is in direct contact with the cooled surface, shows a cellular structure with no visible macro-porosity figure 4.2b. This is the consequence of the initial super-cooling effects, leading to a not steady freezing (Waschkies et al., 2011). The pore gradient characteristics reported here have also been described by several authors

(Moritz & Richter., 2007; Sofie., 2007; Waschkies et al., 2011; Gil-Duran & Ossa., 2016).

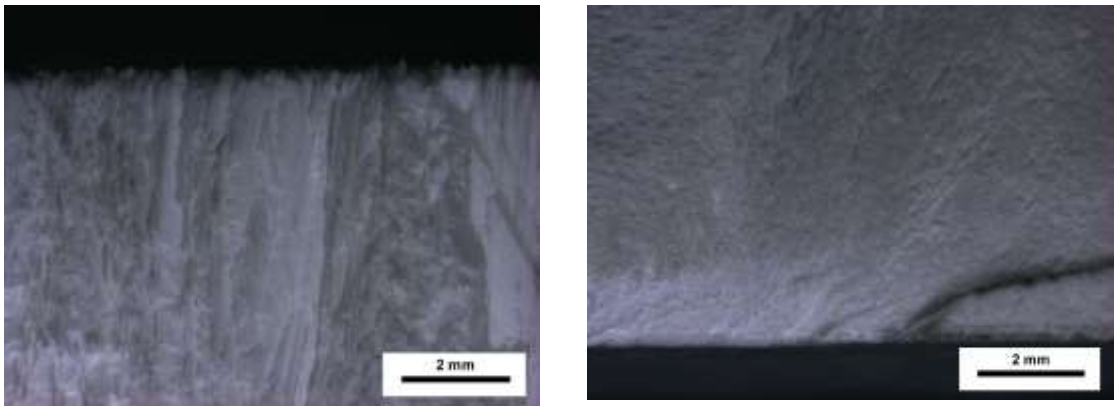

a. b.

Figure 4.2 *Characteristic pore morphology of the sample* ***a.*** *Top* ***b.*** *Bottom. Sample with 30% solid content frozen at 203K in rubber molds of 50 mm x 50 mm.*

Results regarding X-ray computed tomography (CT), Figure 4.3, indicate variations in material density. There are changes in density as a function of sintering temperature and within the sample. Analysis of the cross section of the sample shows that the samples density depends on sintering temperature. Samples sintered at 1773K had the highest average density. Furthermore, density through the sample is not constant. The bottom of the sample shows a denser structure. Towards the top of the sample appears lower density due the well-defined lamellar macro-pores that get wider in the direction of the upper region.

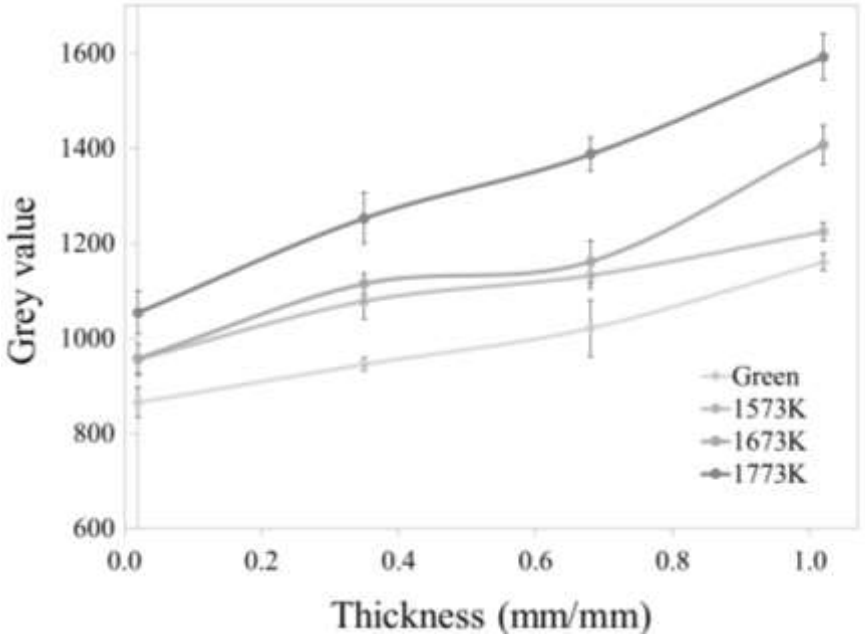

Figure 4.3 *X-ray computed tomography Density gray value at different sintering temperature as a function of thickness.*

The assessment of the effective thermal conductivity (K/K_0) of heterogeneous materials have been extensively studied since the late 19th century (Pietrak & Wiśniewski, 2014). Many models have been proposed based on the materials characteristics. As seen in the current study the pore morphology of materials obtained by freeze casting are lamellar and cellular, each having its own model to predict the thermal conductivity based on pore characteristics (Sumirat et al., 2006). Maxwell's model can be used to predict the thermal conductivity of isolated pores embedded in a continuous matrix, which is a good representation of the cellular porosity of the freeze casted material (Maxwell., 1904). The model is written as follows

$$\frac{K}{K_o} = \frac{2(1-\emptyset)}{(2+\emptyset)} \qquad \textbf{(4.1)}$$

Where ∅ is the volume fraction of pores. On the other hand, the lamellar macro-pores can be regarded as interconnected pores in a continuum matrix. The model that can predict the thermal conductivity is called percolation (Geseleet al., 1997). The percolation model is written as follows

$$\frac{K}{K_o} = (1 - \emptyset)^3 \qquad \textbf{(4.2)}$$

In the perspective of freeze casting pore characteristics, if it is applied a rule of mixtures to combine both models based on the assumption that we can obtain freeze casting materials with different lamellar zone length with respect to total sample length, as will be shown in chapter 5, then the new model can be written as

$$\frac{K}{K_o} = \left(\frac{2(1-\emptyset)}{(2+\emptyset)}\right) F_l + ((1 - \emptyset)^3)(1 - F_l) \qquad \textbf{(4.3)}$$

Where F_l represent the fraction of the material that has lamellar pores. Then, Figure 4.4 illustrates the possible thermal conductivities predicted by each of the models as a function of porosity, and a combination of both lamellar (percolation model) and cellular (Maxwell model). Thus, the freeze casting process provides an opportunity to tune the thermal properties of the bulk sintered material.

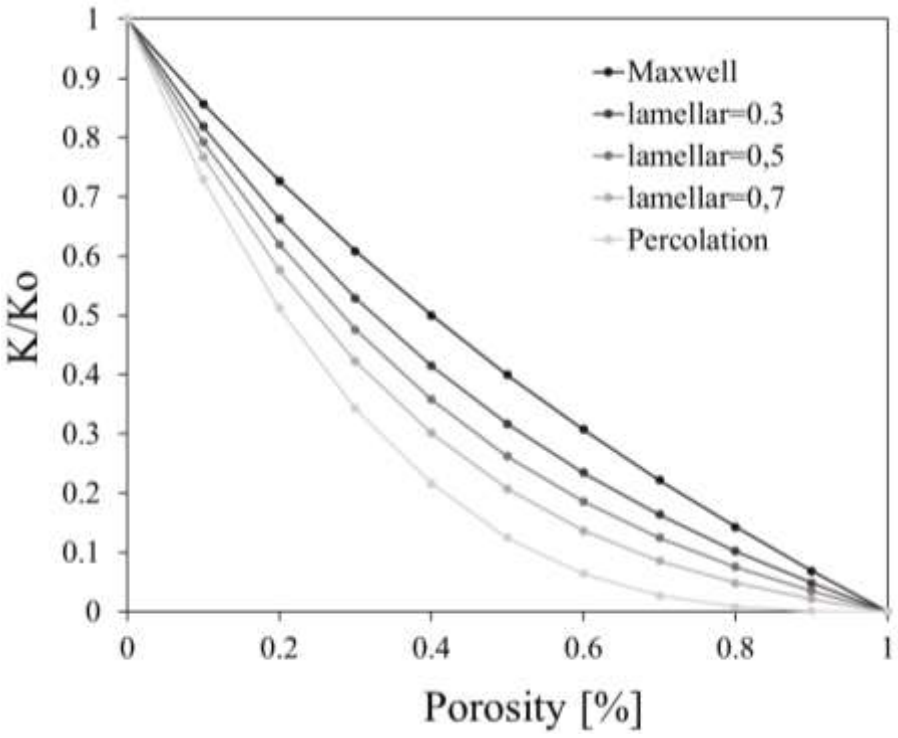

Figure 4.4 *Changes of thermal conductivity as a function of lamellar fraction and total porosity of the sample.*

4.4 Conclusions

Freeze casting process allows materials to be obtained with controlled gradient structures from zones with high density and others with aligned porosity. The freeze casting process is a highly reproducible process giving the opportunity to control the porous structure formation and in consequence providing a prospect to tune the thermal properties of the bulk-sintered material. This process give new tools for the development of new multifunctional materials that combine characteristics that cannot be obtained in a single material manufactured with traditional processing routes.

CHAPTER 5 KAOLIN BASED CERAMICS OBTAINED BY FREEZE CASTING PROCESS

In the current chapter, water-based kaolin suspensions were prepared, varying freezing temperatures and the volume fraction of ceramic particles in the ceramic slurry, aiming at modifying the thermal properties of the slurry domain in order to understand how these influence the cooling patterns and pore morphology of the material.

5.1 Introduction

Materials have different functions in nature. For instance, bone is used in structural applications whereas nacre is used as a protective material. Bioinspired materials are those that mimic one or more aspects of natural materials (Meyers et al., 2013; Chen et al., 2012; Meyers et al., 2008; Launey et al., 2009). In order to obtain bioinspired synthetic materials, scientists have explored different methods of manufacturing, by investigating the scientific report of Malshe et al. (2013) it is possible to find a large list of processes aimed to mimic natural materials features.

Freeze casting offers a tremendous opportunity to mimic some natural structures with synthetic materials that could lead to the development of novel materials for engineering applications. There have been initiatives using freeze casting to produce bioinspired materials for bone replacement (Deville et al., 2006; Yang et al., 2010; Pawelec et al., 2014). Additional studies on freeze casting have

been devoted to the manufacture of parts mimicking some characteristics of nacre with high strength and toughness by infiltrating the structures with a second phase (Munch et al., 2008; Sinchuk et al., 2013; Liu et al., 2014; Shaga et al., 2015). A review article by Hammel et al., (2014) gives a good summary of different applications of porous ceramics.

In general, the freeze casting process consists of four basic steps as it was shown in chapter 2, i) slurry preparation; ii) Solidification; iii) Sublimation, and finally; iv) sintering. To predict the microstructure obtained, an empirical power law dependence of pore characteristics on solidification velocity has been proposed by Deville, (2008). A particular characteristic of the pore defined as wavelength (average width of one pore plus the width of adjacent wall) is predicted by the model upon certain freezing rate. The general conclusion of the model is that increasing the freezing rate decreases the spacing. Moreover, little can be found from literature about how temperature distribution may affect the pore morphology. Thus, the importance of the current chapter is in its delineation of variables like solid content and freezing temperature and how they affect the cooling patterns within the Freeze Casting process. It can open new routes of tuning the microstructure.

5.2 Materials and methods

Freeze casting requires a set of materials to prepare the ceramic slurry. In the current study the aqueous medium used was distilled water as it has been successfully used in previous studies (Launey et al., 2009; Liu, 2011). Kaolin powder with average

particle size of 17.89 µm and specific surface area of 0.569 m^2/g will be used in the current study. Composition of the raw Kaolin powder obtained by X-ray fluorescence is shown in table 5.1 The Kaolin $Al_2Si_2O_5(OH)_4$ employed was obtained from Protokimica S.A.S. The slurry was prepared with different Kaolin contents (10, 30 and 50 %Weighted) to compare how it affect the thermal conductivity and the porosity. The procedure to prepare the ceramic slurry consisted of weighing (Mettler Toledo ML204/1, d=0.1 mg) the precise amount of distilled water, kaolin, and an organic defloculant (polyvinylalcohol, 1.4 wt % of the kaolin powder, 341584 ALDRICH Poly (vinyl alcohol), Mw 89,000-98,000). The organic deflocculant was added to rise the stability of the kaolin suspension via adsorbed organic molecules around the particle surface (Chaiwong & Nuntiya, 2008). Further, Poly(vinyl) alcohol works as a binder, increasing the strength of the green part (Launey et al., 2009). After weighting, the distilled water and organic binder were mixed at 700 RPM in a magnetic stirrer/hot plate (Corning PC-420D) at 80 ºC for a period of 12 hours to dilute the Poly(vinyl alcohol). When this blend reached room temperature (293 K) the ceramic powder was added gradually while kept under constant mixing. To ensure a good dispersion the slurry was mixed for about 24 hours (Liu., 2011).

Table 5.1 *Composition of the raw Kaolin powder obtained by X-ray fluorescence.*

Oxides	**Weight Percentage [%]**
SiO_2	45
Al_2O_3	37
Fe_2O_3	2
Others	3
Mass lost	13

The freezing apparatus used is described in chapter 3. The kaolin slurry was poured into an acrylic mould of 10 mm in diameter, 50 mm in length and thickness of 20 mm. It was cooled at 203K, 143K and 93K, then the average freezing rate was calculated as the length of the sample over the time taken to be frozen. After freezing, the part was freeze dried for 12 hours to allow the ice to sublimate (Preiss et al., 2012) (VirTis BenchTop 4K, 16 mTorr at 193K). Sintering was then performed in a convective furnace (Nabertherm LT 15/13/P330) at 1573K for three hours to ensure densification of the samples. The pore morphology of the samples was assessed by optical microscopy on reflection mode to study the pore morphology (Zeiss Discovery.V8). Finally, the bulk density of the samples was measured using paraffin coating and the Archimedes' method.

Finite Element Analysis (FEA) was used to predict the cooling patterns under different solid content and freezing temperatures (see chapter 3 for model description). The main thermal properties of the ceramic slurry are the thermal diffusivity α, which depends upon the thermal conductivity *k*, the specific heat capacity *Cp* and the mass density ρ of the material. Maxwell, (1881) model was employed to predict the thermal conductivity of solid – liquid mixtures. In addition, the parameter ρCp of the ceramic slurry was estimated using a model proposed by Xuan & Roetzel, (2000).

5.3 Results and discussion

In the pH range of 2–12, the zeta potential is negative so the particles in suspension will tend to repel each other and there will be no tendency for the particles to come together. This behavior is not uncommon for kaolin clays (Chaiwong & Nuntiya., 2008). The kaolin slurry was left at its inner pH 6.0.

The sintered samples showed three well-defined zones as shown in Figure 5.1, each having different pore morphologies. The bottom of the samples show a denser cellular structure with no visible macro-porosity as can be seen in Figure 5.1a. This is the result of the initial super-cooling as it was described in chapter 4 (Waschkies et al., 2011). Just above such zone (Figure 5.1b), there is a transition where the aligned pores begin to get formed, which is produced by the instability of the water crystals while changing from cellular to lamellar structures (Deville et al., 2006). Finally, towards the top of the sample appear well defined lamellar macro-pores that get wider in the

direction of the upper region, as shown in Figure 5.1c. The pores are aligned towards the freezing direction with a branch-like structure. Lamellar macro-pores are the consequence of slower freezing front at the top of the sample resulting in a homogeneous ice nucleation (Schoof et al., 2001). The pore gradient characteristics reported here have also been described by several authors (Moritz & Richter., 2007; Sofie., 2007; Waschkies et al., 2011). As lamellar pores are the most important feature expected from freeze casting, the subsequent analysis will be concentrated on this region.

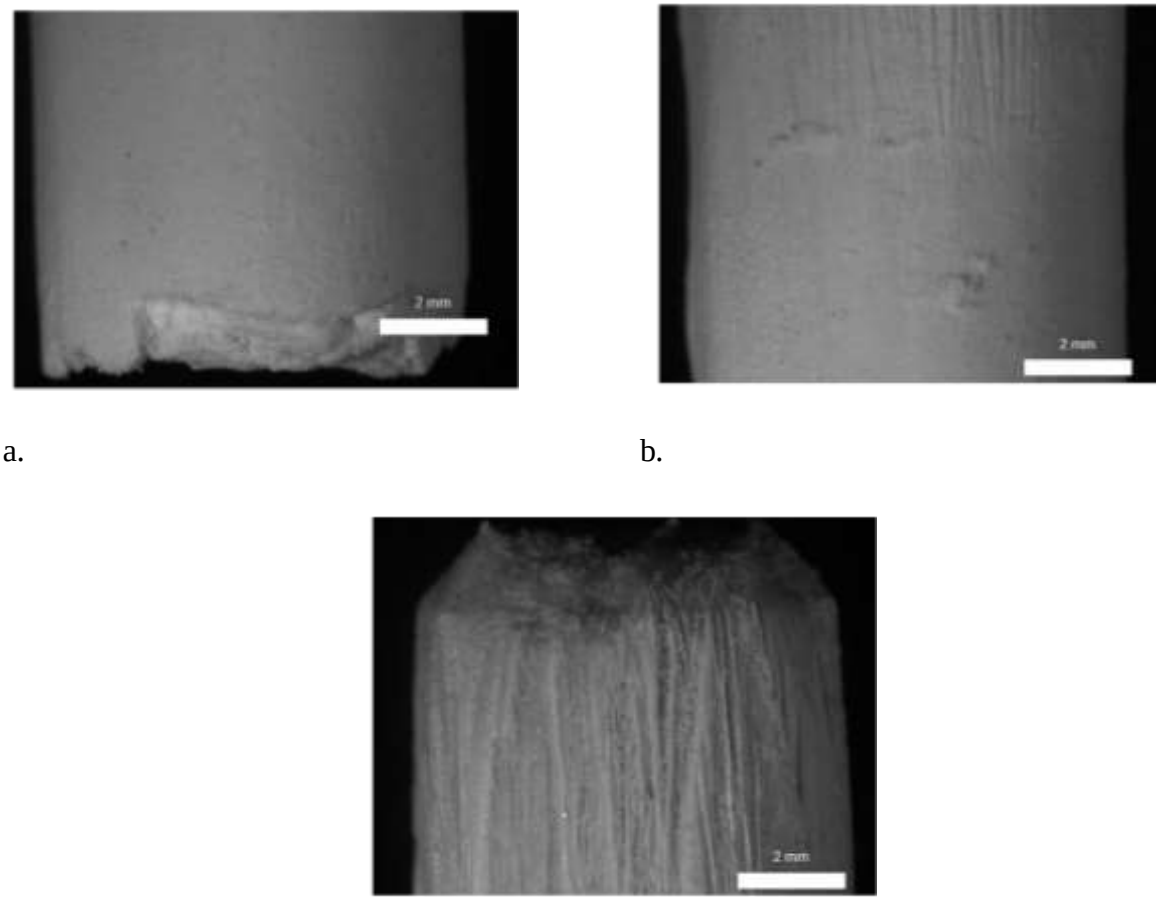

a. b.

c.

Figure 5.1. *Distinctive samples characteristics. a. bottom of the sample. b. transition zone c.*

Top of the sample. Sample prepared with 30% solid content frozen at 203K.

The lengths of the three main regions are dependent on freezing temperature and solid fraction. Different freezing temperatures produce different freezing rates as shown in table 5.2. The length of the lamellar macro-porous region (top of the sample) with respect to the total length of the sample was analyzed, as shown in figure 5.2. In general, slow freezing rates are produced by high freezing temperatures and promote the formation of lamellar structures within the sample, resulting in longer lamellar structures. As freezing temperatures decrease, thus freezing rates increase, and the length of the lamellar structures tend to decrease. Therefore, selecting the appropriate freezing rate has a direct effect on the formation of lamellar structures within the sample.

Table 5.2 *Freezing temperatures and its respective freezing rates.*

Freezing temperature [K]	**Freezing rate [mm/sec]**
203	0,019
143	0,025
93	0,081

Solid fraction also has a direct effect on the length of the lamellar structure. For instance, samples with high solid fractions tend to have a longer lamellar zone at

slow freezing rates, whereas at high freezing rates they show the tendency to have shorter lamellar zones. At 10 % solid content the sintered kaolin part barely forms crystals. At such solid content during freeze-drying, approximately 60% of the poured sample length collapsed due to the lack of interactions between particles. The remaining 40 % of the sample showed the characteristics previously described. Deville et al., (2007) also pointed out that at low ceramic content the green body becomes weaker and difficult to handle. Nonetheless, it can be improved by increasing the binder content. The length and size of the lamellar pores at slow freezing rates at 30 % and 50 % solid fractions are noticeable increased as observed. At 30 % the lamellar pores are well defined along the sample with a remarkable porosity. Higher freezing rates certainly do not promote the formation of well-defined crystals at any solid content. According to Deville et al., (2007) solid fractions higher than 80 wt % make that the lamellar structure get lost and the pores become not interconnected.

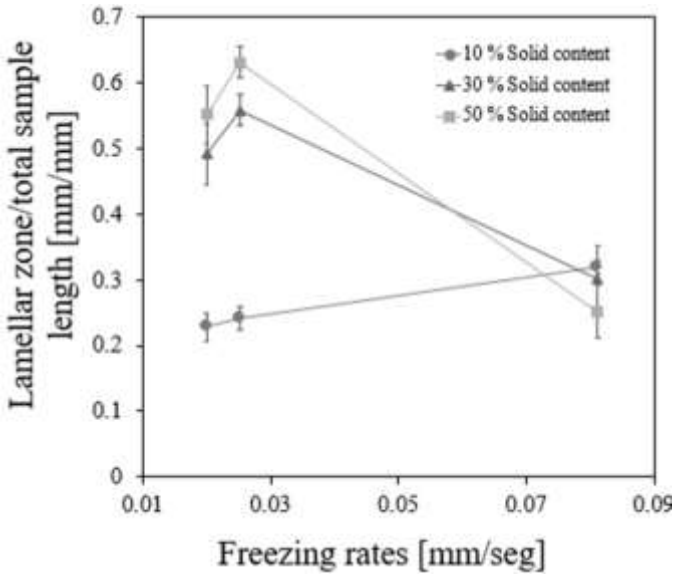

Figure 5.2. *Lamellar zone length with respect to total sample length at different*

freezing rates and solid fractions. The error bars indicate standard deviation.

The thermal properties of particle-fluid mixtures depend on parameters like thermal conductivity of the base fluid and particles, volume fraction and temperature of the system, among others (Wang & Mujumdar., 2007). The thermal conductivity of kaolin clay (0.3 W/m-K) (Etuk et al., 2003) is lower than for water (0.59 W/m-K). Table 5.3 summarizes the thermal conductivity of the ceramic slurry using different solid contents. Higher solid content ends up affecting the thermal conductivity of the ceramic slurry, which slows the freezing front through the sample, resulting in a faster homogeneous ice nucleation, creating longer lamellar structures. The lamellar structure forms as a result of particle-frozen front interactions. Slow freezing rates produce a slow frozen front. Then, the crystals that are forming while the freezing front is advancing are able to move the particles around them, allowing the formation of lamellar structures. On the other hand, high freezing rates do not allow the particles to be moved around the crystal, finishing trapped within the water crystals, hence not permitting the formation of lamellar pores (Rempel & Worster., 1999; Rempel & Worster., 2001). Therefore, selecting the appropriate freezing rate is crucial on the formation of lamellar structures within the sample.

Table 5.3 *Thermal conductivity of ceramic slurry at 10%, 30% and 50% solid content.*

** Calculated with Maxwell, (1881) model.*

Ceramic slurry solid content [%]	**Thermal conductivity [W/m-K] ***
10	0.95
30	0.87
50	0.80

Results of the finite element analysis are shown in figure 5.3. The temperature gradients within the slurry domain are parallel to the freezing direction. During solidification, once the crystal has been formed, ice platelets with a large growth anisotropy are created. The crystals governing the freezing process are the ones whose crystal preferential growth orientation is parallel to the temperature gradient. Crystals that are not oriented in such direction grow at expenses of others. The crystal growth perpendicular to the preferential ice growth axis is between 10^2 to 10^3 times slower, thus lamellar ice crystals with interconnectivity and alignment can be formed when anisotropic freezing is used, leading to the pore characteristics observed (Deville., 2008). Similar explanation has been found for the crystallization of camphene, tertbutyl alcohol and other solvents that provide different types of morphologies (Chen et al., 2012).

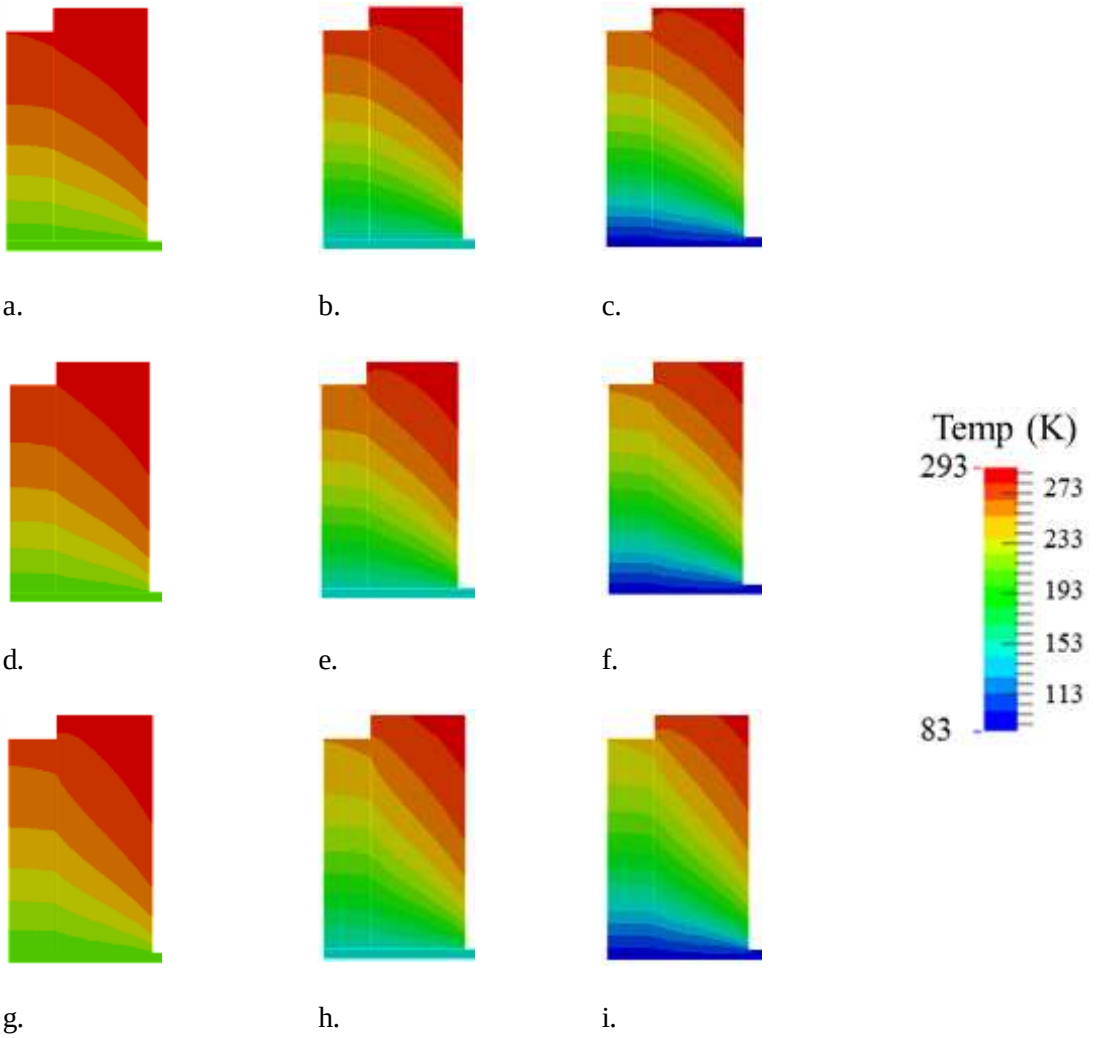

Figure 5.3 *Temperature distribution as function of cooling temperature and solid content a. 203K, b. 143K, c. 93K 10% solid content d. 203K, e. 143K , f. 93K 30% solid content g. 203K , h. 143K, i. 93K 50% solid content.*

Results of density of the lamellar zone at different freezing rates and solid fractions are shown in figure 5.4. Overall, higher solid fractions end up in higher densities of the lamellar structure. Slow freezing rates give time to the particles to sediment, thus the density of the top of the sample tend to be reduced. This feature help explaining the lamellar zone characteristics at different freezing rates and solid

contents. Particle size is an important characteristic to consider when analyzing the microstructure obtained. For instance, Deville et al., (2009) noticed that using submicron particles size results in the formation of crack like defects affecting the compressive strength of the samples. Waschkies et al., (2011) studied the influence of particle size and freezing rates on the microstructure using different alumina particle sizes in a water based polystyrene medium. Results show that when the particles size is around 2µm, lamellar structures are obtained in a wider range of freezing rates (1-1000 µm/s). However, when larger particles (>15µm) are used, lamellar structures are only formed at freezing rates below 3µm/s. Results found in the current study are not in agreement with those by Waschkies et al., (2011). Here, the slowest freezing rate was 19µm/s using an average particle size of 17.886 µm. As mentioned by Deville, (2010) one of the main challenges of comparing freeze casting results is that the pore morphology can be varied by using different additives. For instance, Zhang et al., (2009) observed that the pore morphology and size is significantly affected by the addition of gelatin to the ceramic slurry. Thus, the results obtained here might not match with the ones by Waschkies et al., (2011) because the ceramic slurry were prepared using different base material, medium and additives.

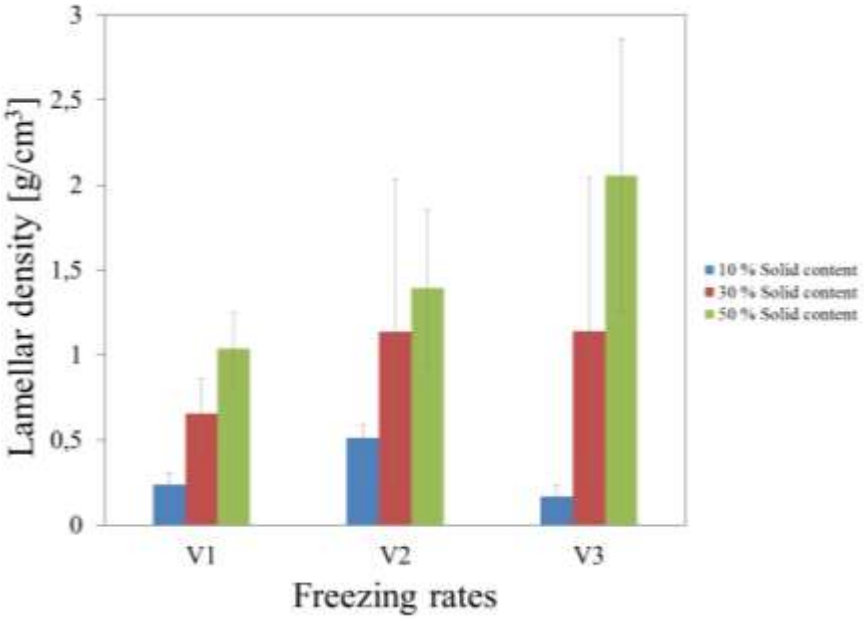

Figure 5.4 *Density of the lamellar zone at different freezing rates and solid content. The error bars indicates the standard deviation.*

5.4 Conclusions

The freeze casting process is a highly reproducible process, giving the opportunity to control the porous structure formation by simply tuning the freezing rates and solid fractions of the slurry. A study of the microstructural characteristics of the samples revealed that varying the solid fraction of ceramic particles and freezing rates have a direct influence on pore morphology.

In general, slow freezing rates promote the formation of lamellar structures at the solid fractions evaluated (10 %, 30 % and 50 %). Nonetheless, the samples showed a lower density due to the sedimentation time given to the particles during the freezing process. The best defined and longer lamellar pores were obtained at 30 % solid

content at slow freezing rates. When the solid fraction is increased to 50% there are still lamellar structures but the samples have a higher density and the lamellar pores are not well defined. At 10 % solid fraction the samples presented several problems during freeze drying due to the lack of particle interactions, as a consequence, the initial poured sample length was reduced about 60% after the freeze drying process. Thus, solid contents as low as 10% are not recommended in freeze casting processes unless such characteristics are desired. Finally, higher freezing rates certainly do not promote the formation of well-defined longer crystals at any solid content evaluated and the samples have higher density.

CHAPTER 6 CONTROL OF POROSITY IN FREEZE CASTING

The aim of this chapter is to test the hypothesis that there is a relationship between the morphological characteristics achieved in the sintered part and the temperature distribution within the Freeze casting process.

6.1 Introduction

Among biological structural materials, bone is exceptional due to its ability to combine strength, stiffness, and toughness with rather limited weight (Currey., 2002). That is largely attributable to its hierarchical microstructure (Meyers et al., 2008). At the macroscale, bone consist of porous structures with interconnectivity, specific aspect ratio, distribution and varying orientations depending on the particular structural requirements (Reznikov et al., 2014).

Scientists have explored the adoption of different manufacturing techniques for developing synthetic materials with controlled porosity (Sellinger et al.,1998; Tang et al., 2003; Seitz et al., 2005; Fu et al., 2011; Li et al., 2012). Among the candidates, freeze casting is a relatively new technique for developing porous materials, which allows control of the pore size and shape through proper control of specific process variables (Li et al., 2012; Deville., 2008; Gutiérrez et al., 2008; Qian & Zhang., 2011; Gil-Durán & Ossa., 2016). The porosity of materials developed by freeze casting have very characteristic microstructures as seen in chapter 2, which can be qualitatively

described as being lamellar, dendritic, cellular, honey comb and/or columnar. Based on the unique qualities of structures available, this process is an excellent candidate for the manufacture of "bone-like" materials or biomaterials with controlled porosity.

The freeze casting process involves four basic steps. Most contributions in this area have argued that the most important step for controlling pore morphology is related with slurry preparation (Scotti & Dunand., 2018). Thus, while the flexibility that is achieved from the range in processing variables is an advantage, it adds significant complexity in understanding the principles that govern porosity-process relationships.

As in freeze casting the pore characteristics are the result of fluid solidification, the driver of the crystal nucleation and growth during freezing is the temperature distribution within the medium as can be inferred from chapter 4. Altogether, freeze casting offers a tremendous opportunity to create synthetic materials that could lead to the development of novel structures for a wide range of applications (Hammel et al., 2014; Liu et al., 2016). Although abundant literature is available about the freeze casting process, the fundamental aspects of ice nucleation and growth, which is the result of atomistic events driven by thermal fluctuations, is far from complete (Karthika et al., 2016; Launey et al., 2009).

Although the freeze casting process is customizable based on setting specific process variables, controlling the development of the pore structure during processing can be challenging (Deville., 2017; Scotti & Dunand., 2018; Algharaibeh et al., 2019). The aim of the current chapter is to test the following hypothesis: the porous morphologies of materials obtained by the Freeze Casting process can be predicted by the temperature gradients during freezing. The objective of this chapter is to evaluate,

by means of numerical modelling and experimentation, the effect of cooling patterns on the porous morphology of freeze casted ceramics. Understanding how these cooling patterns can be used to control the ceramic microstructure in freeze casting will facilitate the manufacture of advanced porous bioinspired structures.

6.2 Materials and Methods

6.2.1 Materials

The ceramic slurry used in this investigation was prepared using distilled water as the aqueous medium. Alumina powder ($Al_2O_3 \geq 99.999\%$) was used as the ceramic material with average particle size of 500 nm (MSESUPPLIES) at 30 wt %. Polyvinylalcohol (341584 ALDRICH, Mw 89,000-98,000) was used as an organic deflocculant at 1.4 wt % of the alumina powder. Poly(vinyl) alcohol works as a binder, increasing the strength of the green part (Launey et al., 2009). The zeta potential of the alumina slurry was measured as a function of pH. The pH of the samples was adjusted to different values from 2 up to 12. The zeta potential measurements were performed using a Malvern Zetasize equipment at room temperature (293.15 K).

Colloidal interactions govern whether the particles in the fluid aggregate or remain separated (Carter & Norton, 2007). The zeta potential characterizes the surface properties of the particles in suspension. The magnitude of this parameter is often used as a measure of the strength of the repulsive interactions between particles. Chemical and physical properties of the particle's surface and medium are affected by its adsorption of polyelectrolytes (Biggs & Healy, 1994), with higher adsorbed

concentrations favoring stability, and low adsorbed concentrations promoting flocculation. The isoelectric point, where the slurry is unstable -and the zeta potential is zero-, was located at pH 2.4 as was observed in chapter 4. Therefore, in order to have particles in suspension before the freezing process, the alumina slurry was kept at pH 6.0, with a zeta potential of -20 mV.

6.2.2 Experimental Methods

Several ceramic materials were manufactured by freeze casting in order to study their porous morphology. All of the samples were manufactured using cylindrical molds with 40 mm inner diameter, 50 mm in height, and with a thickness of the container mold of 5 mm (Figure 6.1). In order to have extremes in thermal conduction and evaluate the effect of thermal properties of the mold on the cooling patterns of the frozen ceramic slurry, two molds were manufactured, one each using rubber (k =1 W/m-K), and Aluminum (k =167 W/m-K). Both were prepared with the same surface finish. In all the cases the base of the mold in contact with the freezing medium was made of aluminum with a thickness of 5 mm (k=167 W/m-K).

Approximately 40 mm of each mold were filled with the alumina slurry. The base of the molds was kept at constant temperatures of either T_1=203.15 K, T_2=143.15 K or T_3=93.15 K to evaluate the effect of the freezing rate on the pore morphology.

After freezing, the samples were subjected to freeze drying for 12 hours to allow sublimation of the ice (VirTis BenchTop 4K, 16 mTorr at 193 K), according to (Preiss et al., 2012). Finally, sintering was performed at 1773.15 K in a convective furnace (Nabertherm LHT 04/17).

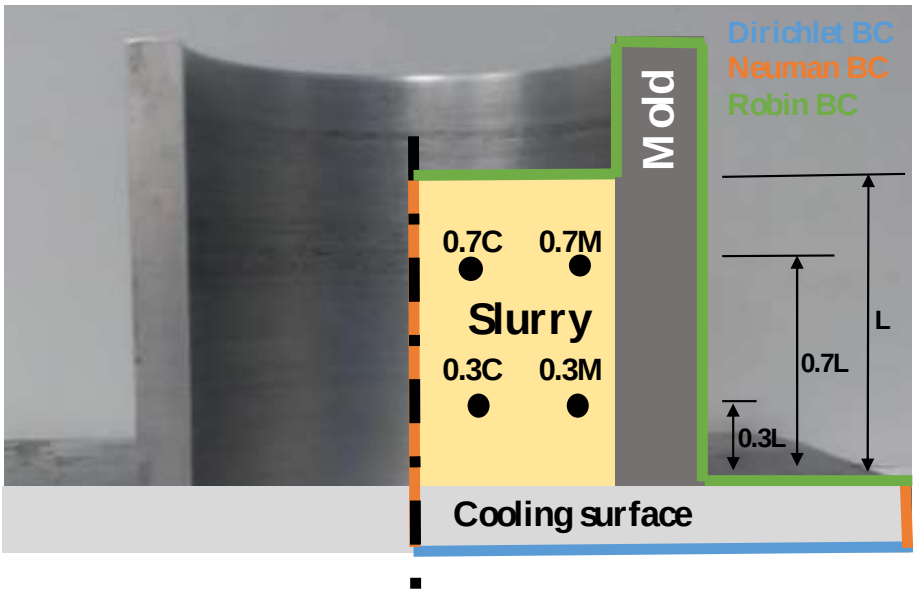

Figure 6.1. *Schematic diagram showing the experimental setup and boundary conditions used in the finite element modeling. The points indicated in the slurry at 0.3L and 0.7L represent positions selected for analysis close to the axis of the slurry (C) and to the mold (M).*

To study the pore morphology and distribution within the samples, optical microscopy (Zeiss, Discovery V8) was performed in reflection mode to measure the effects of variations in the process parameters on pore morphology. Sintered samples were cut in half along the longitudinal direction using a diamond slicing disc. Pore density (λ), defined as the number of pores counted over a 1 mm distance, was measured for the manufactured samples using the magnifications necessary to easily differentiate neighbor pores (i.e.: 60X). Measurements were performed at consistent and specific positions in all samples, corresponding to 0.3L and 0.7L of the mold height as shown in Figure 6.1. A microscopic computed tomography (micro-CT) system (North

Star Imaging X5000) was used to determine porous patterning at macro levels, enabling a quantitative evaluation of distribution at the micro and macro levels. The CT Parameters used for all the scans were Voltage = 80 kV, Current = 600 μA, Geometric Zoom = x8.21, Resolution = ~35.2 μm, number of projections = 1200, frame average = 2, framerate = 1 fps. A phantom-like reference material was not used for calibration. The beam distortion was corrected by an offset and 3 gain maps of the detector in air.

6.2.3 Numerical Methods

Numerical modelling was performed to analyze the temperature distribution within the experimental domain corresponding to the mold and ceramic slurry. The modelling, as seen in chapter 3, consisted of solving the heat equations with given boundary conditions. The freezing device was simplified as shown in chapter 3. The heat transfer problem for simulating freezing within the experimental cylindrical mold is shown in Figure 6.1. The heat equation of this problem is a parabolic partial differential equation. The thermal diffusivity depends on k representing the thermal conductivity, C_p the specific heat capacity and ρ the mass density of the material. The thermal properties of the ceramic slurry depend on various parameters, including the thermal conductivity of the base fluid and particles, volume fraction of particles, surface area, shape of the particles and temperature of the system, among others. There are no theoretical approaches available to predict the thermal properties for the ceramic slurry (Wang, et al., 2007). Nonetheless, there are some semi-empirical correlations that can be used to estimate the thermal conductivity. The classic Maxwell model predicts the thermal conductivity of solid – liquid mixtures (K) based on the thermal conductivity of

the base fluid (*km*), particles (*kp*) -assuming they are spherical- and the volume fraction of particles ø according to (Maxwell, 1881):

$$\frac{K}{km} = 1 + \frac{3\emptyset}{\left(\frac{kp+2\,km}{kp-km}\right)-\emptyset}. \qquad (5.1)$$

Furthermore, the parameter $C_p\ \rho$ for the ceramic slurry was estimated using the approach proposed by Xuan and Roetzel., (2000) following a rule of mixtures. Table 6.1 summarizes the thermal properties of the materials used in the calculations.

Table 6.1 *Thermal properties of the ceramic slurry with 30% solid content, aluminum mold and rubber. * Calculated using (Eq. 3). ** Calculated using Xuan & Roetzel., (2000) model.*

	Thermal conductivity (K) [W/(m•K)]	**Specific heat capacity (Cp) [J/(g•°C)]**	**Mass density (□) [g/cc]**
Aluminum	210	0.9	2.69
Rubber	0.15	0.44	0.95
Ceramic slurry (30% Solid content)	1.856 *	3.945**	
Aluminum oxide	26	0.9	3.8
Water	0.6	4.17	1

A finite element modeling software (Freefem++; v3.57) was employed to simulate the effects of the experimental parameters on the cooling patterns in the ceramic slurry. The parameters specified in the model include the convective coefficient, thermal conductivity of the materials, diameter and thickness of the mold, and temperature at the base of the mold in contact with the cooling plate (e.g. freezing temperature). To compare the effects of varying the control parameters, a pair of points were chosen at two different radial distances from the axis of symmetry, which were located at 0.3L and 0.7L of the total height of the ceramic slurry (Figure 6.1). One set of points was positioned at 5 mm from the axis of symmetry (e.g. 0.3C and 0.7C), and the second was 5 mm away from the mold (e.g. 0.3M and 0.7M). The difference in temperature between the two points (i.e. T_M-T_C) was calculated to evaluate temperature differences at critical zones in the sample domain. A difference in temperature between the points close to zero indicates that there were no temperature differences between the *center* and mold. Alternatively, there were positive or negative differences in temperature.

6.3 Results and discussion

Figure 6.2a shows the microstructural pattern resulting from the freezing process for a sample that was revealed by micro-CT evaluation. In addition, Figure 6.2b shows at higher magnification the lamellar distribution of pores obtained. A comparison of the samples produced by freezing within the two different mold materials is shown in Figure 6.3. Specifically, the samples developed in the Aluminum mold are shown in Figures 6.3a through 6.3c for mold base temperatures of 203K, 143K and 103K,

respectively. Similarly, the samples developed in the rubber mold at these three temperatures are shown in Figures 6.3d through 6.3f, respectively. This general comparison shows that each sample displayed a unique freezing pattern that depended on the cooling temperature and mold material. Nevertheless, the mold material played a substantial role on the freezing patterns as evident from comparing Figures 6.3a-c with 6.3d-f.

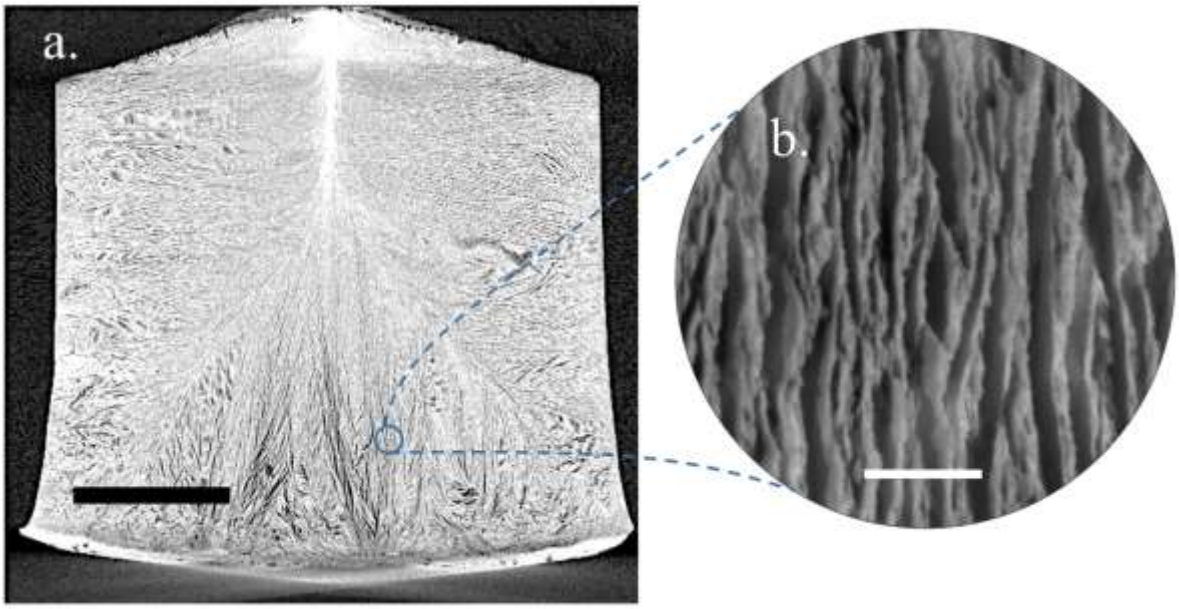

Figure 6.2. *Freeze casted sample manufactured using the aluminum mold at cooling temperature of 203K. a) Micro-CT image; the scale bar represents 10 mm. b) Optical microscopy image showing the lamellar pore morphology; the scale bar represents 500 µm.*

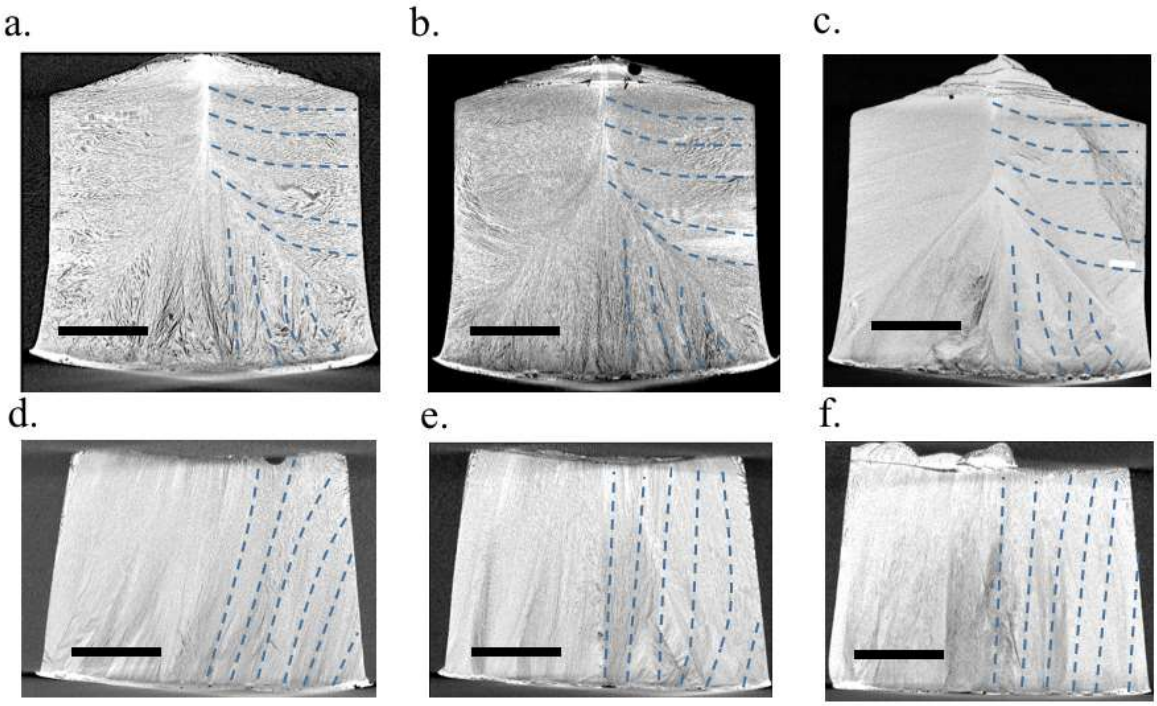

Figure 6.3 *Micro CT images of the freeze casted samples manufactured using the aluminum mold at cooling temperatures of: a) 203K, b) 143K and c) 103K. Corresponding freeze casted samples manufactured using the rubber mold are shown for cooling temperatures of: d) 203K, e) 143K and f) 103K. The blue dashed lines indicate aligned porosity orientations. The scale bar in each figure represents 10 mm. Both aluminum and rubber mold dimensions were of 40 mm inner diameter, height 50 mm and 5 mm of wall thickness.*

Well-defined lamellar macro-pores were observed in all of the samples developed (see Figure. 6.2b). However, they exhibited different particle-frozen front interactions throughout the sample as a consequence of the different freezing temperatures, leading to particular pore morphologies and orientations.

Figure 6.4 shows the variation in the number of pores per millimeter as a function of freezing temperature and position within the samples. Results for the samples fabricated using the aluminum and rubber molds are shown in Figures 6.4a and 6.4b, respectively. Interestingly, for samples prepared using the aluminum mold there were no significant differences in pore distribution when comparing the two slurry positions (e.g.: 0.3L and 0.7L), as shown in Figure 6.4a. However, the cooling temperature does have an important effect on pore density; smaller pores resulted when the mold temperature driving the freezing process is reduced. On the other hand, for samples prepared using the rubber mold, there were significant differences in the pore density as a function of distance from the cooling plate, and in terms of the freezing temperature, as shown in Figure 6.4b.

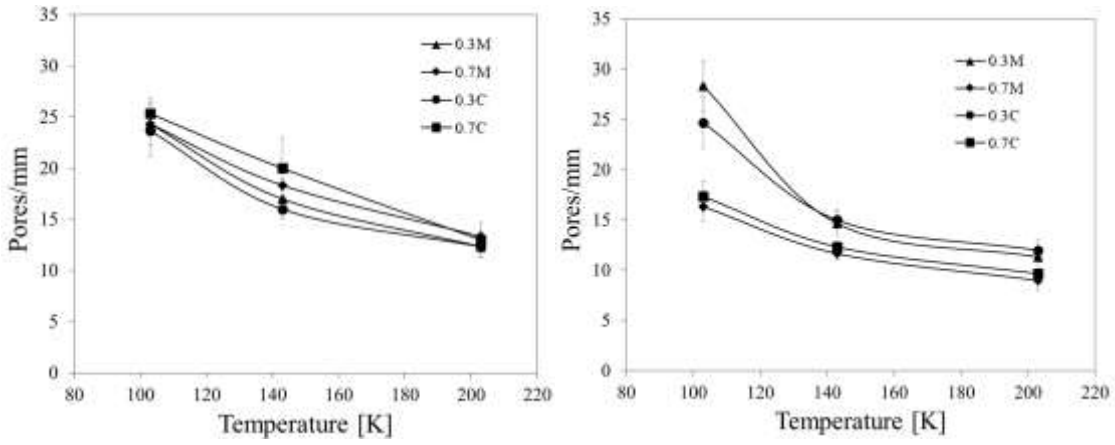

Figure 6.4 *Measured variation of pore density (Pores/mm) as a function of freezing temperature for different positions within the freeze casted samples. a) Aluminum mold; b) Rubber mold.*

Figure 6.5 shows the effect of varying mold geometry on the FEA results. For instance, as shown in Figure 6.5a, increasing the mold wall thickness from 4 mm to 45 mm results in a reduction of the temperature difference in the slurry domain between the center and mold region at the two points of evaluation (0.3L and 0.7L). Furthermore, there is a mold thickness value (15 mm), which causes a remarkable change in the slope of the curve. From that point on, increasing the mold wall thickness does not cause a substantial change in temperature difference. Moreover, as shown in Figure 6.5b, the mold can also be tuned to control the slurry temperature differences through adjustment of the mold diameter. As the diameter of the mold is reduced from approximately 60

mm, a more even cooling distribution is obtained as evident in Figure 6.5b. In general, the mold design can be tuned to achieve a particular cooling pattern and microstructural texture.

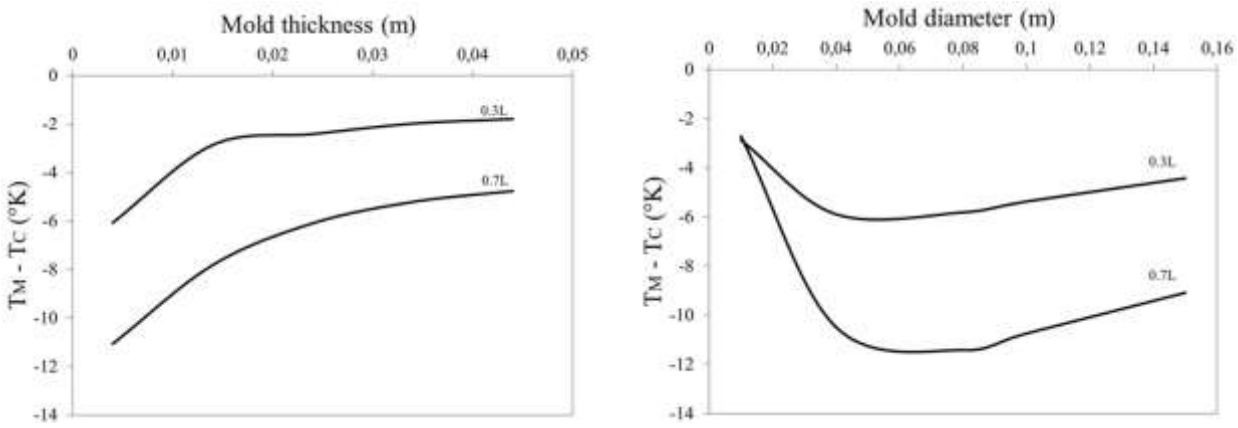

a. b.

Figure 6.5 *Effect of mold geometry on temperature differences calculated using the FEA. a) mold thickness; b) mold internal diameter.*

Figure 6.6 shows the effects of the thermal parameters on the temperature differences at the points of interest based on the FEM. Specifically, the importance of the freezing temperature, convective coefficient and thermal conductivity are shown in Figures 6.6a through 6.6c, respectively. As evident in Figure 6.6a, the freezing temperature is shown to have a linear effect on the temperature difference between the points of interest and as the freezing temperature increases more uniform cooling patterns are obtained. External variables can also have an effect on the cooling patterns. For instance, the air speed around the mold, which is represented by the convective coefficient, has an important effect on temperature differences as shown in Figure 6.6b.

A higher convective coefficient promotes larger differences in temperature (Figure 6.6b). This parameter is easy to adjust in the manufacturing process to control the morphology of pores in the sample. On the other hand, Figure 6.6c shows the effect of the mold thermal conductivity between 1 W/m-K (i.e. rubber) and 167 W/m-K (i.e. aluminum) on the temperature difference between the points of interest. As evident from the response, the thermal conductivity of the mold material directly influences the cooling patterns obtained. That is also apparent from the solidification patterns in Figure 6.3. Molds with higher thermal conductivities promote faster freezing of the slurry near the mold wall than at the center (Figures 6.3a – 6.3c). Furthermore, for a thermal conductivity of approximately 5 W/m-K the difference in temperature between the two points is a minimum, which results in an even cooling pattern and leads to a horizontal temperature gradient.

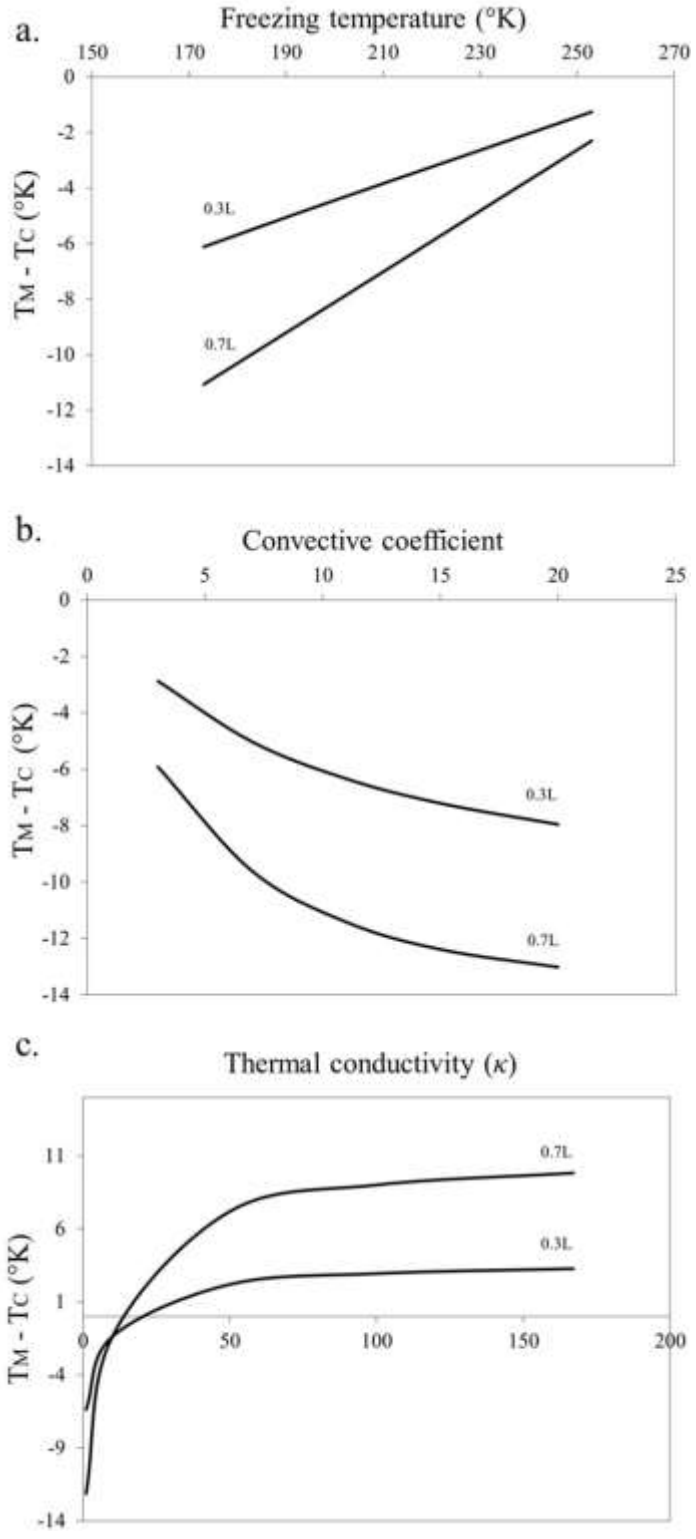

Figure 6.6 *Effect of thermal variables on temperature differences as calculated using the FEA. a) freezing temperature; b) convective coefficient; c) thermal conductivity.*

Figure 6.7 shows the temperature distributions in the mold as a function of the freezing temperature using both rubber and aluminum molds. Results for the Aluminum mold and the rubber mold are shown at three different temperatures (203K, 143K and 93K) in Figures 6.7a – 6.7c and Figure 6.7d – 6.7f, respectively. There are clear differences in the cooling patterns within the experimental domains for each mold material. For a given mold material, the cooling gradients have the same orientation respect to the freezing direction. Nevertheless, the differences in temperature range with freezing temperature are significant.

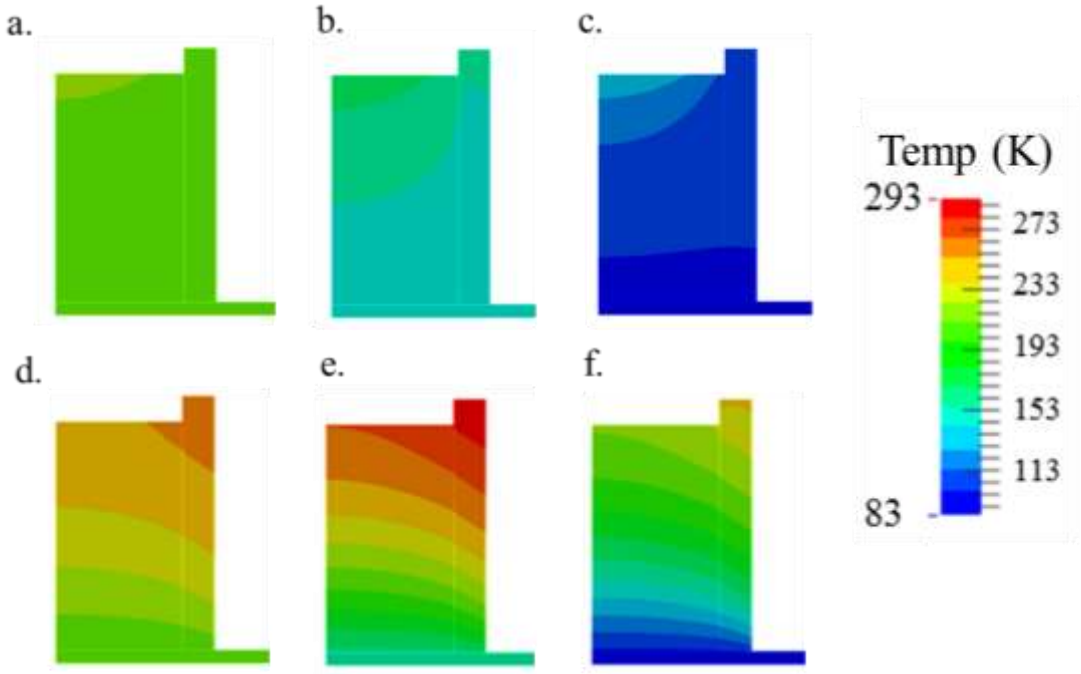

Figure 6.7 *Calculated temperature differences with varying molds and freezing temperatures. Aluminum mold: a) 203K; b) 143K; c) 93K. Rubber mold: d) 203K; e) 143K; f) 93K.*

Solidification is a critical stage in the freeze casting process since the crystal morphology determines the resulting pore characteristics. While there are different crystal structures that can be formed with water-based slurries (Boettinger et al., 2000), hexagonal ice crystals are the most common (Deville.,2008). During the phase transition of liquid water to ice, the disordered liquid molecules become organized via hydrogen bonding on a process that can be divided into nucleation and crystal growth, both having an impact in the crystals formed (Hobbs., 2010). During nucleation, water molecules are initially organized to form the solid that will undergo growth to form the crystals. The nucleation process is primarily stochastic and cannot be completely controlled (Matsumoto et al., 2002; Ayel et al., 2006). Once it has occurred, the newly formed nuclei undergo a process called secondary nucleation, which leads to the development of new crystals (Myerson., 2002; Flemings., 1974). After this initial nucleation, the remaining liquid undergoes crystal growth (Rey & May, 2004).

There are two preferential axes of crystal growth, including the *a* and *c* axes, with the *c-axis* growing 10^{-2}-10^{-3} slower than the *a-axis* (Boettinger et al., 2000). The *a-axis* is parallel to the temperature gradient, establishing the orientation of the main crystals in such directions, while the *c-axis* crystal growth is perpendicular to the temperature gradients, promoting interconnectivity between crystals and resulting in pore interconnectivity in the final cast material (Figure 6.8).

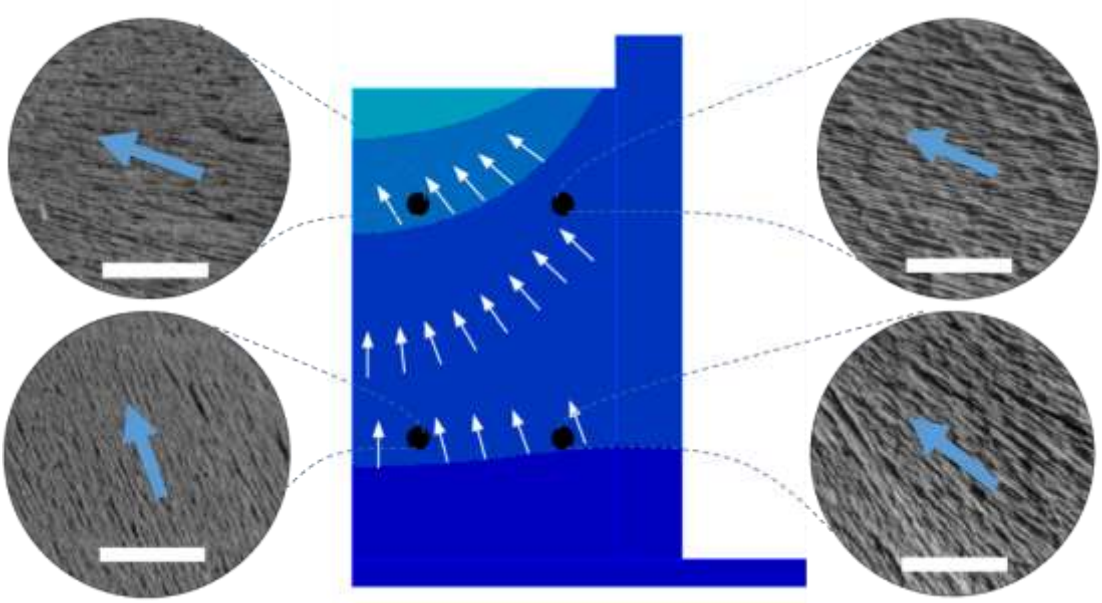

a.

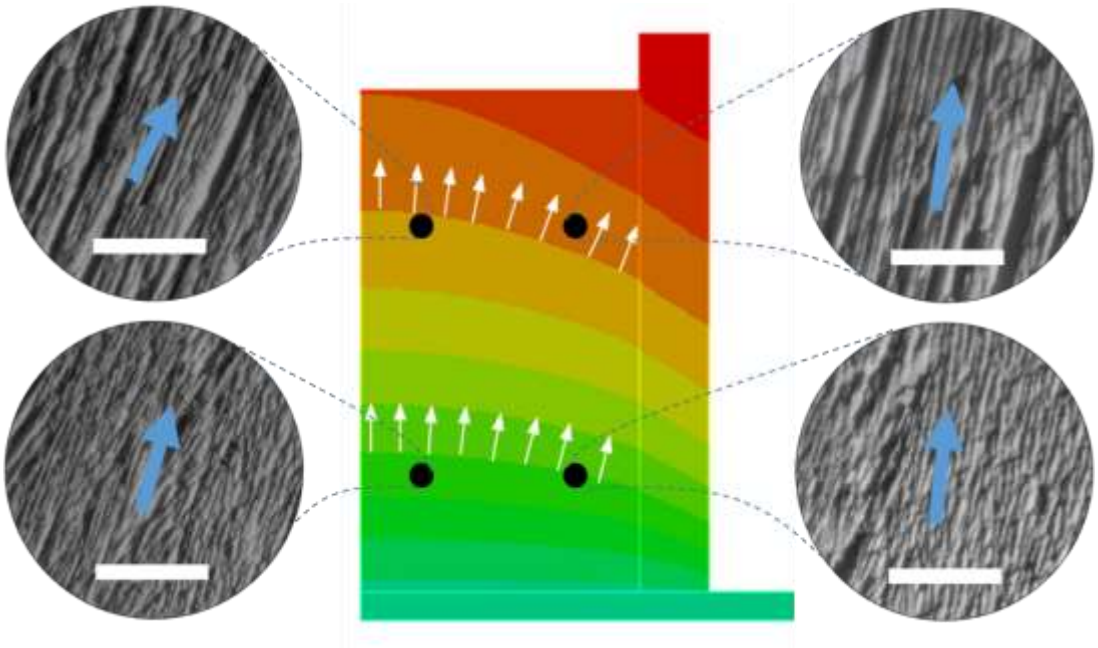

b.

Figure 6.8 *Relation between temperature gradients and pore orientation for a) Aluminum mold with freezing temperature of 93K. b) Rubber mold with freezing temperature of 143K. The arrows indicate the direction of temperature gradient and a-axis of crystal growth. The scale bar represents 1mm.*

The mechanisms driving crystal growth explains why there are no significant differences in pore density as a function of position in the freeze castings produced using the aluminum mold. With this mold the temperature tends to be homogenized close to the walls due to its high thermal conductivity. On the other hand, higher temperature gradients were found at 0.3L and 0.7L with the rubber mold as a consequence of its thermal insulating nature. Therefore, if there is a large mismatch between the thermal properties of the ceramic slurry and mold, horizontal temperature gradients will develop, affecting the growth kinetics of the crystals and the pore characteristics of the material obtained. Thus, the temperature gradients and their orientation can be chosen to develop a desired pore structure. Figure 6.8 shows the influence of temperature gradients on the pore orientation. Note that the freeze casting shows pore orientations that depend on the specific thermal properties of the mold material and the position analyzed. The orientation of the pores is governed by - and aligned with - the temperature gradients as indicated by the arrows in the Figure. Thus, when a complex pore morphology is to be produced by freeze casting, the temperature gradients have to be considered in the mold design.

The variables affecting the cooling patterns within freeze castings have been described and it has been shown how specific mold and thermal variables affect the cooling patterns within the slurry domain, and their effect on the pore morphology. Alumina was used in this chapter as a material with known properties and characteristics. Different parameters like zeta potential, thermal properties, sedimentation, particle size and morphology have to be considered if a different material is going to be used. However, if these parameters are correctly controlled in the

slurry and the numerical model include the main thermal parameters and dimensional conditions of the mold used, it is expected that the temperature gradients can be correctly predicted and hence the final pore morphology of the part fabricated.

6.4 Conclusions

A combined experimental and numerical study was conducted to characterize the cooling patterns obtained during solidification in freeze casting and contributions from the primary process parameters. It was found that the freezing pattern and cast microstructure are strongly dependent on the mold design and temperature gradient, which affect the pore morphology of the cast material. Temperature gradients within the mold domain are controlled by the sample volume, shape, freezing rate, convective coefficient and mold material and geometry. Finite element modeling served as a tool to understand the temperature gradients quantitatively and their contribution to the pore morphology. A porous structure with required morphology can be obtained via tuning of the temperature gradients during freezing of the slurry through careful control of the dimensional and thermal properties of the mold.

CHAPTER 7 CONCLUSIONS AND FUTURE WORK

This chapter summarizes the main conclusions of this dissertation:

The aim of the current thesis was to test the hypothesis that the physical properties of the material obtained by the Freeze Casting process can be predicted by the cooling patterns during freezing. A combined experimental and numerical study was conducted to characterize the cooling patterns obtained during solidification in freeze casting and contributions from the primary process parameters. Furthermore, solid fraction of ceramic particles and freezing rates were evaluated. In Freeze Casting process the pore characteristics are a result of the fluid solidification, the driver of the crystal development during freezing are the temperature distribution within the slurry.

Regarding solid content of the ceramic slurry and freezing temperatures, it was shown that high freezing temperatures promote the formation of lamellar structures. The best defined and longer lamellar pores were obtained at 30 % solid content at high freezing temperatures. When the solid fraction is increased to 50% there are still lamellar structures and the samples have a higher density but the lamellar pores are not well defined. At 10 % solid fraction the samples presented several problems during freeze drying due to the lack of particle interactions, as a consequence the initial poured sample length was reduced about 60% after the freeze drying process. Moreover, low freezing temperatures certainly do not promote the formation of well-defined longer crystals at any solid content evaluated and the lamellar structure of the samples have

higher density. Results also showed that sedimentation may be used as a tuning tool to create gradient structures.

Ice nucleation and growth are driven by thermal fluctuations during freezing, resulting in a particular pore morphology and distribution within the final material. It was shown that a simple heat transfer model efficiently and reliably predict the temperature evolution during freezing, gaining a better understanding of fundamental aspects of ice nucleation and growth driven by the cooling patterns. Finite element modeling served as a tool to understand the temperature gradients quantitatively and their contribution to the pore morphology. A porous structure with required morphology can be obtained via tuning of the temperature gradients during freezing of the slurry through careful control of the dimensional and thermal properties of the mold.

It was found that the freezing pattern and the final microstructure are strongly dependent on the mold design and temperature gradient, which affect the pore morphology of the material. Temperature gradients within the mold domain are controlled by the sample volume, shape, freezing rate, convective coefficient and mold material and geometry. Freeze casting process allows materials to be obtained with controlled gradient structures from zones with high density and others with aligned porosity. The freeze casting process is a reproducible process giving the opportunity to control the porous structure formation and in consequence providing a prospect to tune the thermal properties of the bulk-sintered material. This process gives new tools for the development of new multifunctional materials that can combine characteristics that cannot be obtained in a single material manufactured with traditional processing routes.

Finally, the future work arising from the current thesis is deeper analysis of the use of Finite Element Analysis to help guide mold design and the thermal conditions necessary to achieve a desired pore morphology. It is worth noting that if finer details are required to be predicted, a more elaborated 3D problem with multiphasic model including dynamics of crystal growth and changes in volume has to be developed. Nonetheless, a simple model like the one presented here can lead to a realistic control of the porosity orientation in freeze cast materials and can be used to manufacture bioinspired porous materials.

References

Algharaibeh, S., Ireland, A. J., & Su, B. (2019). Bi-directional freeze casting of porous alumina ceramics: A study of the effects of different processing parameters on microstructure. *Journal of the European Ceramic Society*, *39*(2-3), 514-521.

Arai, N., & Faber, K. T. (2019). Hierarchical porous ceramics via two-stage freeze casting of preceramic polymers. *Scripta Materialia*, *162*, 72-76.

Ayel, V., Lottin, O., Faucheux, M., Sallier, D., & Peerhossaini, H. (2006). Crystallisation of undercooled aqueous solutions: Experimental study of free dendritic growth in cylindrical geometry. *International journal of heat and mass transfer*, *49*(11-12), 1876-1884.

Bai, H., Wang, D., Delattre, B., Gao, W., De Coninck, J., Li, S., & Tomsia, A. P. (2015). Biomimetic gradient scaffold from ice-templating for self-seeding of cells with capillary effect. *Acta biomaterialia*, 20, 113-119.

Biggs S. & Healy T.W. (1994). Electrosteric stabilization of colloidal zirconia with low molecular weight polyacrylic-acid - an atomic-force microscopy study. *Journal of the Chemical Society- Faraday Transactions*, , 90(22), 3415-3421

Blindow, S., Pulkin, M., Koch, D., Grathwohl, G., & Rezwan, K. (2009). Hydroxyapatite/SiO2 composites via freeze casting for bone tissue engineering. *Advanced Engineering Materials*, 11(11), 875-884.

Boettinger, W. J., Coriell, S. R., Greer, A. L., Karma, A., Kurz, W., Rappaz, M., & Trivedi, R. (2000). Solidification microstructures: recent developments, future directions. *Acta materialia*, *48*(1), 43-70.

Bouville, F., Maire, E., & Deville, S. (2014). Lightweight and stiff cellular ceramic structures by ice templating. *Journal of Materials Research*, 29(2), 175-181.

Carter, C.B. and Norton, M.G., 2013, Ceramic Materials: Science & Engineering. *Ed, Springer*. 2nd Edition.

Cesarano J, Aksay I. A, Bleier A. (1988). Stability of aqueous alpha-Al2O3 suspensions with poly(methacrylic acid) poly-electrolyte. *Journal of the American Ceramic Society*, 1988, 71(4), 250-255.

Chaiwong, N. & Nuntiya, A. (2008) Influence of pH, electrolytes and polymers on flocculation of kaolin particle. *Science*, 35 (1), 11-16.

Chen, P.Y., McKittrick, J. & Meyers, M.A. (2012) Biological materials: functional adaptations and bioinspired designs. *Progress in Materials Science*, 57 (8), 1492-1704.

Chen, Z., Liu, X., Shen, T., Wu, C., & Zhang, L. (2020). Template-assisted freeze casting of macroporous Ti6Al4V scaffolds with long-range order lamellar structure. *Materials Letters*, 127374.

Chu, Y., Lu, Z., Li, J., Zhu, Y., Zhang, S., & Chen, J. (2015). Preparation of poly (L-lactic acid) with aligned structures by unidirectional freezing. *Polymers for Advanced Technologies*, 26(6), 606-612.

Currey, J. D. (2002). Bones: structure and Mechanics Princeton University Press: Princeton. *NJ, USA*.

Delattre, B., Bai, H., Ritchie, R. O., De Coninck, J., & Tomsia, A. P. (2013). Unidirectional freezing of ceramic suspensions: In situ X-ray investigation of the effects of additives. *ACS applied materials & interfaces*, 6(1), 159-166.

Deville, S. (2008). Freeze-casting of porous ceramics: a review of current achievements and issues. *Advanced Engineering Materials*, 10(3), 155-169.

Deville, S. (2010). Freeze-casting of porous biomaterials: structure, properties and opportunities. *Materials*, 3(3), 1913-1927.

Deville, S. (2017). Freezing colloids: natural and technological occurrences. In *Freezing Colloids: Observations, Principles, Control, and Use* (pp. 1-46). Springer, Cham.

Deville S & Bernard-Granger G. (2010). Influence of surface tension, osmotic pressure and pores morphology on the densification of ice-templated ceramic. *Journal of the European Ceramic Society* . l12. 121.

Deville, S., Maire, E., Bernard-Granger, G., Lasalle, A., Bogner, A., Gauthier, C., Guizard, C. (2009). Metastable and unstable cellular solidification of colloidal suspensions. *Nature materials*, 8(12), 966-972.

Deville, S., Saiza, E., Nalla, R.K., Tomsiaa, A.P. (2006). Freezing as a path to build complex composites. *Science*. 311, 515–518.

Deville, S., Saiz, E., & Tomsia, A. P. (2007). Ice-templated porous alumina structures. *Acta Materialia*, 55(6), 1965-1974

Deville, S., Viazzi, C., Leloup, J., Lasalle, A., Guizard, C., Maire, E., ... & Gremillard, L. (2011). Ice shaping properties, similar to that of antifreeze proteins, of a zirconium acetate *complex. PloS one*, 6(10), e26474.

Eisenberg, D., & Kauzmann, W. (2005). *The structure and properties of water*. Oxford University Press on Demand.

Etuk, S. E., Akpabio, I. O., & Udoh, E. M. (2003). Comparison of the thermal properties of clay samples as potential walling material for naturally cooled building design. *Journal of Environmental Sciences,* 15(1), 65-68.

Flauder, S., Heinze, T., & Müller, F. A. (2014). Cellulose scaffolds with an aligned and open porosity fabricated via ice-templating. *Cellulose*, *21*(1), 97-103.

Flemings, M. C. (1974). Solidification processing. *Metallurgical transactions*, 5(10), 2121-2134.

Frank, G., Christian, E., & Dietmar, K. (2011). A Novel Production Method for Porous SoundAbsorbing Ceramic Material for HighTemperature Applications. *International Journal of Applied Ceramic Technology*, 8(3), 646-652.

Fu Q; Saiz E; Tomsia A.P. (2011). Bioinspired strong and highly porous glass scaffolds. *Advanced Functional Materials*. 21.1058-1063.

Fukushima, M., & Yoshizawa, Y. I. (2014). Fabrication of highly porous silica thermal insulators prepared by gelation–freezing route. *Journal of the American Ceramic Society*, 97(3), 713-717.

Fukushima, M., & Yoshizawa, Y. I. (2016). Fabrication and morphology control of highly porous mullite thermal insulators prepared by gelation freezing route. Journal of the European Ceramic Society, 36(12), 2947-2953.

Gesele, G., Linsmeier, J., Drach, V., Fricke, J., & Arens-Fischer, R. (1997). Temperature-dependent thermal conductivity of porous silicon. *Journal of Physics D: Applied Physics*, *30*(21), 2911.

Gil-Durán, S., & Ossa, E. A. (2016). Kaolin based ceramics obtained by Freeze casting process. *Ingeniería y competitividad*, *18*(2), 133-140.

Gil-Duran, S., Arola, D., & Ossa, E. A. (2020) Control of Porosity in Freeze Casting. *JOM*, 1-10.

Gutiérrez, M. C., Ferrer, M. L., & del Monte, F. (2008). Ice-templated materials: sophisticated structures exhibiting enhanced functionalities obtained after unidirectional freezing and ice-segregation-induced self-assembly†. *Chemistry of Materials*, 20(3), 634-648.

Hammel, E. C., Ighodaro, O. R., & Okoli, O. I. (2014). Processing and properties of advanced porous ceramics: An application based review. *Ceramics International*, *40*(10), 15351-15370.

Hautcoeur, D., Lorgouilloux, Y., Leriche, A., Gonon, M., Nait-Ali, B., Smith, D. S., ... & Cambier, F. (2016). Thermal conductivity of ceramic/metal composites from preforms produced by freeze casting. Ceramics International, 42(12), 14077-14085.

Hobbs, P. V. (2010). *Ice physics*. Oxford university press.

Husmann, A., Pawelec, K., Burdett, C., Best, S., & Cameron, R. (2015). Numerical simulations to determine the influence of mould design on ice-templated scaffold structures. *genesis*, *6*, 8.

Ishizaki, K., Komarneni, S., & Nanko, M. (2013). Porous Materials: Process technology and applications (Vol. 4). Springer science & business media.

James, F., & Doremus, R. (2008). Ceramic and glass materials: Structure, properties and processing. Editorial Springer, Nueva York, EUA, 56-62.

Jing, Z. E. N. G., Zhang, Y., Zhou, K. C., & Zhang, D. (2014). Effects of alcohol additives on pore structure and morphology of freeze-cast ceramics. *Transactions of Nonferrous Metals Society of China*, 24(3), 718-722.

Karthika, S., Radhakrishnan, T. K., & Kalaichelvi, P. (2016). A review of classical and nonclassical nucleation theories. *Crystal Growth & Design*, *16*(11), 6663-6681.

Kitaoka, S., Matsushima, Y., Chen, C., & Awaji, H. (2004). Thermal cyclic fatigue behavior of porous ceramics for gas cleaning. *Journal of the American Ceramic Society*, 87(5), 906-913.

Knrpnrnrcr, R. J. (1975). Crystal growth from the melt: a review. *Am Mineral*, 60, 798-814.

Kristen L. S. & David C. D, (2018). Freeze casting – A review of processing, microstructure and properties via the open data repository, FreezeCasting.net. *Progress in Materials Science.* 94. 243-305

Kumaraswamy, G., Biswas, B., & Choudhury, C. K. (2016). Colloidal assembly by ice templating. *Faraday discussions*, 186, 61-76.

Launey, M.E., Munch, E., Alsem, D.H., Barth, H.B., Saiz, E., Tomsia, A.P. & Ritchie, R.O. (2009). Designing highly toughened hybrid composites through nature-inspired hierarchical complexity. *Acta Materialia,* 57 (10), 2919-2932.

Lewis J.A. (2000). Colloidal processing of ceramics. *Journal of the American Ceramic Society*, 83(10), 2341-2359.

Lewis, R. W., Morgan, K., Thomas, H. R., & Seetharamu, K. N. (1996). *The finite element method in heat transfer analysis*. John Wiley & Sons.

Li, D., & Li, M. (2012). Porous Y2SiO5 ceramic with low thermal conductivity. Journal of Materials Science & Technology, 28(9), 799-802.

Li, W. L., Lu, K., & Walz, J. Y. (2012). Freeze casting of porous materials: review of critical factors in microstructure evolution. *International materials reviews*, *57*(1), 37-60.

Lichtner, A. Z., Jauffrès, D., Roussel, D., Charlot, F., Martin, C. L., & Bordia, R. K. (2015). Dispersion, connectivity and tortuosity of hierarchical porosity composite

SOFC cathodes prepared by freeze-casting. *Journal of the European Ceramic Society*, 35(2), 585-595.

Liu, G. (2011) Fabrication of porous ceramics and composites by a novel freeze casting process. Ph.D. thesis, School of metallurgy and materials, *University of Birmingham, Birmingham,* United Kingdom.

Liu, G., & Button, T. W. (2013). The effect of particle size in freeze casting of porous alumina–zirconia composite. *Ceramics International*, 39(7), 8507-8512.

Liu, Q., Ye, F., Gao, Y., Liu, S., Yang, H., & Zhou, Z. (2014). Fabrication of a new SiC/2024Al co-continuous composite with lamellar microstructure and high mechanical properties. *Journal of Alloys and Compounds*, 585, 146-153.

Liu, R., Xu, T., & Wang, C. A. (2016). A review of fabrication strategies and applications of porous ceramics prepared by freeze-casting method. *Ceramics International*, 42(2), 2907-2925.

Liu, X., Xue, W., Shi, C., & Sun, J. (2015). Fully interconnected porous Al2O3 scaffolds prepared by a fast cooling freeze casting method. *Ceramics International*, 41(9), 11922-11926.

Macchettaa, A., Turner, I.G., Bowena, C.R. (2009). Fabrication of HA/TCP scaffolds with a graded and porous structure using a camphene-based freeze-casting method. *Acta Biomaterials*. 5, 1319–27.

Mallick, K. K., & Winnett, J. (2012). Preparation and characterization of porous Bioglass® and PLLA scaffolds for tissue engineering applications. *Journal of the American Ceramic Society*, 95(9), 2680-2686.

Malshe, A., Rajurkar, K., Samant, A., Hansen, H.N., Bapat, S. & Jiang, W. (2013). Bio-inspired functional surfaces for advanced applications. *CIRP Annals-Manufacturing Technology,* 62 (2), 607-628.

Matsumoto, M., Saito, S., & Ohmine, I. (2002). Molecular dynamics simulation of the ice nucleation and growth process leading to water freezing. *Nature*, 416(6879), 409.

Maxwell, J. C. (1881). *A treatise on electricity and magnetism* (Vol. 1). Clarendon press.

Maxwell-Garnett, J. C. (1904). Colours in metal glasses and in metallic films. *Phil. Trans. R. Soc. Lond, A, 203,* 385-420.

Meyers, M. A., Chen, P. Y., Lin, A. Y. M., & Seki, Y. (2008). Biological materials: structure and mechanical properties. *Progress in Materials Science*, *53*(1), 1-206.

Meyers, M.A., Lin, A.Y.M., Chen, P.Y. & Muyco, J. (2008). Mechanical strength of abalone nacre: role of the soft organic layer. *Journal of the Mechanical behavior of biomedical materials,* 1 (1), 76-85.

Meyers, M.A., McKittrick, J. & Chen, P.Y. (2013). Structural biological materials: critical mechanics-materials connections. *Science,* 339 (6121), 773-779.

Moon, J. W., Hwang, H. J., Awano, M., & Maeda, K. (2003). Preparation of NiO–YSZ tubular support with radially aligned pore channels. *Materials Letters*, 57(8), 1428-1434.

Moritz, T., & Richter, H. J. (2007). Ice-mould freeze casting of porous ceramic components. *Journal of the European Ceramic Society*, 27(16), 4595-4601.

Munch, E., Launey, M.E., Alsem, D.H., Saiz, E., Tomsia, A.P. & Ritchie, R.O. (2008). Tough, bio-inspired hybrid materials. *Science*, 322 (5907), 1516-1520.

Munch, E., Saiz, E., Tomsia, A. P., & Deville, S. (2009). Architectural control of freeze-cast ceramics through additives and templating. *Journal of the American Ceramic Society*, 92(7), 1534-1539.

Myerson, A. (2002). *Handbook of industrial crystallization*. Butterworth-Heinemann.

Naebe, M., & Shirvanimoghaddam, K. (2016). Functionally graded materials: A review of fabrication and properties. *Applied Materials Today*, *5*, 223-245.

Naleway, S. E., Christopher, F. Y., Porter, M. M., Sengupta, A., Iovine, P. M., Meyers, M. A., & McKittrick, J. (2015). Bioinspired composites from freeze casting with clathrate hydrates. *Materials & Design*, 71, 62-67.

Naviroj, M., Wang, M. M., Johnson, M. T., & Faber, K. T. (2017). Nucleation-controlled freeze casting of preceramic polymers for uniaxial pores in Si-based ceramics. *Scripta Materialia*, 130, 32-36.

Okaji, R., Sakashita, S., Tazumi, K., Taki, K., Nagamine, S., & Ohshima, M. (2013). Interconnected pores on the walls of a polymeric honeycomb monolith structure created by the unidirectional freezing of a binary polymer solution. *Journal of Materials Science*, 48(5), 2038-2045.

Onna, D., Minaberry, Y., & Jobbágy, M. (2015). Hierarchical bioglass scaffolds: introducing the “milky way” for templated bioceramics. *Journal of Materials Chemistry B*, 3(15), 2971-2977.

Oosthuizen P. H & Naylor D. (1999). An Introduction to Convective Heat Transfer Analysis. *McGraw Hill*. 19-20

Pagano, E., Chinelatto, A. S. A., & Chinelatto, A. L. (2020). Freeze casting process for the generation of graded porosity in Al2O3 ceramics. *Cerâmica*, *66*(377), 65-73.

Pawelec, K. M., Husmann, A., Best, S. M., & Cameron, R. E. (2014). Ice-templated structures for biomedical tissue repair: From physics to final scaffolds. *Applied Physics Reviews*, 1(2), 021301.

Pawelec, K. M., Husmann, A., Best, S. M., & Cameron, R. E. (2015). Altering crystal growth and annealing in ice-templated scaffolds. *Journal of materials science*, *50*(23), 7537-7543.

Peko, C., Groth, B., & Nettleship, I. (2010). The effect of polyvinyl alcohol on the microstructure and permeability of freeze-cast alumina. *Journal of the American Ceramic Society*, 93(1), 115-120.

Pekor, C. M., Kisa, P., & Nettleship, I. (2008). Effect of Polyethylene Glycol on the Microstructure of Freeze-Cast Alumina. *Journal of the American Ceramic Society*, 91(10), 3185-3190.

Pekor, C., & Nettleship, I. (2014). The effect of the molecular weight of polyethylene glycol on the microstructure of freeze-cast alumina. *Ceramics International*, *40*(7), 9171-9177.

Pham-Huu, C., Bouchy, C., Dintzer, T., Ehret, G., Estournes, C., & Ledoux, M. J. (1999). High surface area silicon carbide doped with zirconium for use as catalyst support. Preparation, characterization and catalytic application. *Applied Catalysis A: General*, 180(1), 385-397

Pietrak, K., & Wiśniewski, T. S. (2014). A review of models for effective thermal conductivity of composite materials. Journal of Power Technologies, 95(1), 14-24.

Plucknett, K. P., Quinlan, M., Garrido, L., & Genova, L. (2008). Microstructural development in porous β-Si3N4 ceramics prepared with low volume RE2O3–MgO–(CaO) additions (RE= La, Nd, Y, Yb). *Materials Science and Engineering: A*, *489*(1-2), 337-350.

Porter, M. M., Yeh, M., Strawson, J., Goehring, T., Lujan, S., Siripasopsotorn, P., ... & McKittrick, J. (2012). Magnetic freeze casting inspired by nature. *Materials Science and Engineering: A*, *556*, 741-750.

Preiss, A., Su, B., Collins, S. & Simpson, D. (2012). Tailored graded pore structure in zirconia toughened alumina ceramics using double-side cooling freeze casting. *Journal of the European Ceramic Society* 32 (8), 1575-1583.

Qian, L., Ahmed, A., Foster, A., Rannard, S. P., Cooper, A. I., & Zhang, H. (2009). Systematic tuning of pore morphologies and pore volumes in macroporous materials by freezing. *Journal of Materials Chemistry*, 19(29), 5212-5219.

Qian L & Zhang H.F. (2011). Controlled freezing and freeze drying: a versatile route for porous and micro-nano-structured materials. *Journal of Chemical Technology and Biotechnology*.86.172.

Rempel, A. & Worster, M. (2001). Particle trapping at an advancing solidification front with interfacial-curvature effects. *Journal of Crystal Growth*, 223 (3), 420-432.

Rey, L., & May, J. C. (2004). *Freeze-Drying/Lyophilization Of Pharmaceutical & Biological Products, Revised and Expanded*. CRC Press.

Reznikov, N., Shahar, R., & Weiner, S. (2014). Bone hierarchical structure in three dimensions. *Acta biomaterialia*, *10*(9), 3815-3826.

Rouhollahi, A., Ilegbusi, O., Florczyk, S., Xu, K., & Foroosh, H. (2019). Effect of Mold Geometry on Pore Size in Freeze-Cast Chitosan-Alginate Scaffolds for Tissue Engineering. *Annals of biomedical engineering*, 1-13.

Sadik, C., El Amrani, I. E., & Albizane, A. (2014). Recent advances in silica-alumina refractory: A review. Journal of Asian Ceramic Societies, 2(2), 83-96.

Schoof, H., Apel, J., Heschel, I., & Rau, G. (2001). Control of pore structure and size in freeze-dried collagen sponges. Journal of biomedical materials research, 58(4), 352-357.

Scotti, K. L., & Dunand, D. C. (2018). Freeze casting–A review of processing, microstructure and properties via the open data repository, FreezeCasting. net. *Progress in Materials Science*, *94*, 243-305.

Seitz H; Rieder W; Irsen S; Leukers B; Tille C. (2005). Three-dimensional printing of porous ceramic scaffolds for bone tissue engineering. Journal of *Biomedical Materials Research Part B: Applied Biomaterials*.74.782-788.

Sellinger A; Weiss P.M; Nguyen A; LuY.F; Assink R.A;GongW.L; Brinker. (1998). Continuous self-assembly of organic-inorganic nanocomposite coatings that mimic nacre.*Nature*.394, 256-260.

Seuba, J., Leloup, J., Richaud, S., Deville, S., Guizard, C., & Stevenson, A. J. (2017). Fabrication of ice-templated tubes by rotational freezing: Microstructure, strength, and permeability. *Journal of the European Ceramic Society*, 37(6), 2423-2429.

Shaga, A., Shen, P., Sun, C., & Jiang, Q. (2015). Lamellar-interpenetrated Al–Si–Mg/SiC composites fabricated by freeze casting and pressure less infiltration. *Materials Science and Engineering: A*, 630, 78-84.

Shanmugam, K., Radhakrishnan, T. K., & Kalaichelvi, P. (2016). A Review on Classical and Non Classical Nucleation Theories. *Crystal Growth & Design*. 16 (11), 6663-668.

Sinchuk, Y., Roy, S., Gibmeier, J., Piat, R., & Wanner, A. (2013). Numerical study of internal load transfer in metal/ceramic composites based on freeze-cast ceramic preforms and experimental validation. *Materials Science and Engineering: A*, 585, 10-16.

Sobolev, S. L. (2012). Rapid colloidal solidifications under local nonequilibrium diffusion conditions. *Physics Letters A*, 376(47-48), 3563-3566.

Sofie, S. W. (2007). Fabrication of Functionally Graded and Aligned Porosity in Thin Ceramic Substrates With the Novel Freeze–Tape-Casting Process. *Journal of the American Ceramic Society*, 90(7), 2024-2031.

Sofie, S. W., & Dogan, F. (2001). Freeze casting of aqueous alumina slurries with glycerol. *Journal of the American Ceramic Society*, 84(7), 1459-1464.

Souza, D. F., Nunes, E. H., Pimenta, D. S., Vasconcelos, D. C., Nascimento, J. F., Grava, W., ... & Vasconcelos, W. L. (2014). Synthesis and structural evaluation of freeze-cast porous alumina. *Materials Characterization*, 96, 183-195.

Studart, A. R., Gonzenbach, U. T., Tervoort, E., & Gauckler, L. J. (2006). Processing routes to macroporous ceramics: a review. *Journal of the American Ceramic Society*, *89*(6), 1771-1789.

Sumirat, I., Ando, Y., & Shimamura, S. (2006). Theoretical consideration of the effect of porosity on thermal conductivity of porous materials. *Journal of Porous Materials*, *13*(3-4), 439-443.

Szepes, A., Ulrich, J., Farkas, Z., Kovács, J., & Szabó-Révész, P. (2007). Freeze-casting technique in the development of solid drug delivery systems. *Chemical Engineering and Processing: Process Intensification*, 46(3), 230-238.

Tang, Y., Zhao, K., Hu, L., & Wu, Z. (2013). Two-step freeze casting fabrication of hydroxyapatite porous scaffolds with bionic bone graded structure. *Ceramics International*, *39*(8), 9703-9707.

Tang, Z., Kotov, N. A., Magonov, S., & Ozturk, B. (2003). Nanostructured artificial nacre. *Nature materials*, *2*(6), 413.

Ulrike G.K; Wegst M.S ; Amalie E.D; Philipp M.H. (2010). Biomaterials by freeze casting. *Philosophical Transactions of the Roya lSociety A.* 368. 2099–2121.

Wang, N., Liu, Y., Zhang, Y., Du, Y., & Zhang, J. (2019). Control of pore structure during freeze casting of porous SiC ceramics by different freezing modes. *Ceramics International*, *45*(9), 11558-11563.

Wang, X. Q., & Mujumdar, A. S. (2007). Heat transfer characteristics of nanofluids: a review. *International journal of thermal sciences*, *46*(1), 1-19.

Waschkies, T., Oberacker, R., & Hoffmann, M. J. (2011). Investigation of structure formation during freeze-casting from very slow to very fast solidification velocities. *Acta Materialia*, 59(13), 5135-5145.

Wegst, U. G., Schecter, M., Donius, A. E., & Hunger, P. M. (2010). Biomaterials by freeze casting. *Philosophical Transactions of the Royal Society A: Mathematical, Physical and Engineering Sciences*, *368*(1917), 2099-2121.

Wilson, P. W., Heneghan, A. F., & Haymet, A. D. J. (2003). Ice nucleation in nature: supercooling point (SCP) measurements and the role of heterogeneous nucleation. *Cryobiology*, 46(1), 88-98.

Wu, J., Liu, X., Yan, L., & Zhang, L. (2017). Long-range order and preferred orientation in WS2 scaffold created by freeze casting. *Materials Letters*, 196, 414-418.

Wu, J., Luo, B., Liu, X., & Zhang, L. (2018). Control of the structure and mechanical property of porous WS2 scaffold during freeze casting. *Journal of Porous Materials*, 25(1), 37-43.

Xu, T., & Wang, C. A. (2015). Grain Orientation and Domain Configuration in 3-1 Type Porous PZT Ceramics with Ultrahigh Piezoelectric Properties. *Journal of the American Ceramic Society*, 98(9), 2700-2702.

Xuan, Y., & Roetzel, W. (2000). Conceptions for heat transfer correlation of nanofluids. *International Journal of heat and Mass transfer*, *43*(19), 3701-3707.

Yang, H., Ye, F., Liu, Q., Liu, S., Gao, Y., & Liu, L. (2015). A novel silica aerogel/porous Si 3 N 4 composite prepared by freeze casting and sol-gel impregnation with high-performance thermal insulation and wave-transparent. *Materials Letters*, 138, 135-138

Yang, T.Y., Lee, J.M., Yoon, S.Y. & Park, H.C. (2010). Hydroxyapatite scaffolds processed using a TBA-based freeze-gel casting/polymer sponge technique. *Journal of Materials Science: Materials in Medicine,* 21 (5), 1495-1502.

Yang, T. Y., Yoon, S. Y., Lee, G. D., Wang, C. A., Stevens, R., Huang, Y., & Park, H. C. (2005). Freeze casting of aqueous Al2O3/Y-TZP slurries. *In Key Engineering Materials.* 280, 1065-1068.

Zhang, R., Qu, Q., Han, B., & Wang, B. (2016). A novel silica aerogel/porous Y2SiO5 ceramics with low thermal conductivity and enhanced mechanical properties prepared by freeze casting and impregnation. Materials Letters, 175, 219-222.

Zhang, Y., Xie, M., Roscow, J., Bao, Y., Zhou, K., Zhang, D., & Bowen, C. R. (2017). Enhanced pyroelectric and piezoelectric properties of PZT with aligned porosity for energy harvesting applications. *Journal of Materials Chemistry A*, 5(14), 6569-6580.

Zhang, Y., Zuo, K., & Zeng, Y. P. (2009). Effects of gelatin addition on the microstructure of freeze-cast porous hydroxyapatite ceramics. *Ceramics International*, 35(6), 2151-2154.

Zuo, K. H., Zeng, Y. P., & Jiang, D. (2008). Properties of Microstructure-Controllable Porous Yttria-Stabilized Ziroconia Ceramics Fabricated by Freeze Casting. *International Journal of Applied Ceramic Technology*, 5(2), 198-203.

Zuo, K. H., Zeng, Y. P., & Jiang, D. (2010). Effect of polyvinyl alcohol additive on the pore structure and morphology of the freeze-cast hydroxyapatite ceramics. *Materials Science and Engineering*: C, 30(2), 283-287.

Zou, Y., Gaudillere, C., Escribano, J. E., Serra, J. M., & Malzbender, J. (2017). Microstructure, mechanical behavior and flow resistance of freeze-cast porous 3YSZ substrates for membrane applications. *Journal of the European Ceramic Society*, 37(9), 3167-3176.